CrossMark

First Search for Gravitational Waves from Known Pulsars with Advanced LIGO

B. P. Abbott[1], R. Abbott[1], T. D. Abbott[2], M. R. Abernathy[3], F. Acernese[4,5], K. Ackley[6], C. Adams[7], T. Adams[8], P. Addesso[9], R. X. Adhikari[1], V. B. Adya[10], C. Affeldt[10], M. Agathos[11], K. Agatsuma[11], N. Aggarwal[12], O. D. Aguiar[13], L. Aiello[14,15], A. Ain[16], P. Ajith[17], B. Allen[10,18,19], A. Allocca[20,21], P. A. Altin[22], A. Ananyeva[1], S. B. Anderson[1], W. G. Anderson[18], S. Appert[1], K. Arai[1], M. C. Araya[1], J. S. Areeda[23], N. Arnaud[24], K. G. Arun[25], S. Ascenzi[15,26], G. Ashton[10], M. Ast[27], S. M. Aston[7], P. Astone[28], P. Aufmuth[19], C. Aulbert[10], A. Avila-Alvarez[23], S. Babak[29], P. Bacon[30], M. K. M. Bader[11], P. T. Baker[31], F. Baldaccini[32,33], G. Ballardin[34], S. W. Ballmer[35], J. C. Barayoga[1], S. E. Barclay[36], B. C. Barish[1], D. Barker[37], F. Barone[4,5], B. Barr[36], L. Barsotti[12], M. Barsuglia[30], D. Barta[38], J. Bartlett[37], I. Bartos[39], R. Bassiri[40], A. Basti[20,21], J. C. Batch[37], C. Baune[10], V. Bavigadda[34], M. Bazzan[41,42], C. Beer[10], M. Bejger[43], I. Belahcene[24], M. Belgin[44], A. S. Bell[36], B. K. Berger[1], G. Bergmann[10], C. P. L. Berry[45], D. Bersanetti[46,47], A. Bertolini[11], J. Betzwieser[7], S. Bhagwat[35], R. Bhandare[48], I. A. Bilenko[49], G. Billingsley[1], C. R. Billman[6], J. Birch[7], R. Birney[50], O. Birnholtz[10], S. Biscans[1,12], A. Bisht[19], M. Bitossi[34], C. Biwer[35], M. A. Bizouard[24], J. K. Blackburn[1], J. Blackman[51], C. D. Blair[52], D. G. Blair[52], R. M. Blair[37], S. Bloemen[53], O. Bock[10], M. Boer[54], G. Bogaert[54], A. Bohe[29], F. Bondu[55], R. Bonnand[8], B. A. Boom[11], R. Bork[1], V. Boschi[20,21], S. Bose[16,56], Y. Bouffanais[30], A. Bozzi[34], C. Bradaschia[21], P. R. Brady[18], V. B. Braginsky[49,153], M. Branchesi[57,58], J. E. Brau[59], T. Briant[60], A. Brillet[54], M. Brinkmann[10], V. Brisson[24], P. Brockill[18], J. E. Broida[61], A. F. Brooks[1], D. A. Brown[35], D. D. Brown[45], N. M. Brown[12], S. Brunett[1], C. C. Buchanan[2], A. Buikema[12], T. Bulik[62], H. J. Bulten[11,63], A. Buonanno[29,64], D. Buskulic[8], C. Buy[30], R. L. Byer[40], M. Cabero[10], L. Cadonati[44], G. Cagnoli[65,66], C. Cahillane[1], J. Calderón Bustillo[44], T. A. Callister[1], E. Calloni[5,67], J. B. Camp[68], M. Canepa[46,47], K. C. Cannon[69], H. Cao[70], J. Cao[71], C. D. Capano[10], E. Capocasa[30], F. Carbognani[34], S. Caride[72], J. Casanueva Diaz[24], C. Casentini[15,26], S. Caudill[18], M. Cavaglià[73], F. Cavalier[24], R. Cavalieri[34], G. Cella[21], C. B. Cepeda[1], L. Cerboni Baiardi[57,58], G. Cerretani[20,21], E. Cesarini[15,26], S. J. Chamberlin[74], M. Chan[36], S. Chao[75], P. Charlton[76], E. Chassande-Mottin[30], B. D. Cheeseboro[31], H. Y. Chen[77], Y. Chen[51], H.-P. Cheng[6], A. Chincarini[47], A. Chiummo[34], T. Chmiel[78], H. S. Cho[79], M. Cho[64], J. H. Chow[22], N. Christensen[61], Q. Chu[52], A. J. K. Chua[80], S. Chua[60], S. Chung[52], G. Ciani[6], F. Clara[37], J. A. Clark[44], F. Cleva[54], C. Cocchieri[73], E. Coccia[14,15], P.-F. Cohadon[60], A. Colla[28,81], C. G. Collette[82], L. Cominsky[83], M. Constancio, Jr.[13], L. Conti[42], S. J. Cooper[45], T. R. Corbitt[2], N. Cornish[84], A. Corsi[72], S. Cortese[34], C. A. Costa[13], M. W. Coughlin[61], S. B. Coughlin[85], J.-P. Coulon[54], S. T. Countryman[39], P. Couvares[1], P. B. Covas[86], E. E. Cowan[44], D. M. Coward[52], M. J. Cowart[7], D. C. Coyne[1], R. Coyne[72], J. D. E. Creighton[18], T. D. Creighton[87], J. Cripe[2], S. G. Crowder[88], T. J. Cullen[23], A. Cumming[36], L. Cunningham[36], E. Cuoco[34], T. Dal Canton[68], S. L. Danilishin[36], S. D'Antonio[15], K. Danzmann[10,19], A. Dasgupta[89], C. F. Da Silva Costa[6], V. Dattilo[34], I. Dave[48], M. Davier[24], G. S. Davies[36], D. Davis[35], E. J. Daw[90], B. Day[44], R. Day[34], S. De[35], D. DeBra[40], G. Debreczeni[38], J. Degallaix[65], M. De Laurentis[5,67], S. Deléglise[60], W. Del Pozzo[45], T. Denker[10], T. Dent[10], V. Dergachev[29], R. De Rosa[5,67], R. T. DeRosa[7], R. DeSalvo[91], J. Devenson[50], R. C. Devine[31], S. Dhurandhar[16], M. C. Díaz[87], L. Di Fiore[5], M. Di Giovanni[92,93], T. Di Girolamo[5,67], A. Di Lieto[20,21], S. Di Pace[28,81], I. Di Palma[28,29,81], A. Di Virgilio[21], Z. Doctor[77], V. Dolique[65], F. Donovan[12], K. L. Dooley[73], S. Doravari[10], I. Dorrington[94], R. Douglas[36], M. Dovale Álvarez[45], T. P. Downes[18], M. Drago[10], R. W. P. Drever[1], J. C. Driggers[37], Z. Du[71], M. Ducrot[8], S. E. Dwyer[37], T. B. Edo[90], M. C. Edwards[61], A. Effler[7], H.-B. Eggenstein[10], P. Ehrens[1], J. Eichholz[1], S. S. Eikenberry[6], R. A. Eisenstein[12], R. C. Essick[12], Z. Etienne[31], T. Etzel[1], M. Evans[12], T. M. Evans[7], R. Everett[74], M. Factourovich[39], V. Fafone[14,15,26], H. Fair[35], S. Fairhurst[94], X. Fan[71], S. Farinon[47], B. Farr[77], W. M. Farr[45], E. J. Fauchon-Jones[94], M. Favata[95], M. Fays[94], H. Fehrmann[10], M. M. Fejer[40], A. Fernández Galiana[12], I. Ferrante[20,21], E. C. Ferreira[13], F. Ferrini[34], F. Fidecaro[20,21], I. Fiori[34], D. Fiorucci[30], R. P. Fisher[35], R. Flaminio[65,96], M. Fletcher[36], H. Fong[97], S. S. Forsyth[44], J.-D. Fournier[54], S. Frasca[28,81], F. Frasconi[21], Z. Frei[98], A. Freise[45], R. Frey[59], V. Frey[24], E. M. Fries[1], P. Fritschel[12], V. V. Frolov[7], P. Fulda[6,68], M. Fyffe[7], H. Gabbard[10], B. U. Gadre[16], S. M. Gaebel[45], J. R. Gair[99], L. Gammaitoni[32], S. G. Gaonkar[16], F. Garufi[5,67], G. Gaur[100], V. Gayathri[101], N. Gehrels[68], G. Gemme[47], E. Genin[34], A. Gennai[21], J. George[48], L. Gergely[102], V. Germain[8], S. Ghonge[17], Abhirup Ghosh[17], Archisman Ghosh[11,17], S. Ghosh[11,53], J. A. Giaime[2,7], K. D. Giardina[7], A. Giazotto[21], K. Gill[103], A. Glaefke[36], E. Goetz[10], R. Goetz[6], L. Gondan[98], G. González[2], J. M. Gonzalez Castro[20,21], A. Gopakumar[104], M. L. Gorodetsky[49], S. E. Gossan[1], M. Gosselin[34], R. Gouaty[8], A. Grado[5,105], C. Graef[36], M. Granata[65], A. Grant[36], S. Gras[12], C. Gray[37], G. Greco[57,58], A. C. Green[45], P. Groot[53], H. Grote[10], S. Grunewald[29], G. M. Guidi[57,58], X. Guo[71], A. Gupta[16], M. K. Gupta[89], K. E. Gushwa[1], E. K. Gustafson[1], R. Gustafson[106], J. J. Hacker[23], B. R. Hall[56], E. D. Hall[1], G. Hammond[36], M. Haney[104], M. M. Hanke[10], J. Hanks[37], C. Hanna[74], J. Hanson[7], T. Hardwick[2], J. Harms[57,58], G. M. Harry[3], I. W. Harry[29], M. J. Hart[36], M. T. Hartman[6], C.-J. Haster[45,97], K. Haughian[36], J. Healy[107], A. Heidmann[60], M. C. Heintze[7], H. Heitmann[54], P. Hello[24], G. Hemming[34], M. Hendry[36], I. S. Heng[36], J. Hennig[36], J. Henry[107], A. W. Heptonstall[1], M. Heurs[10,19], S. Hild[36], D. Hoak[34], D. Hofman[65], K. Holt[7], D. E. Holz[77], P. Hopkins[94], J. Hough[36], E. A. Houston[36], E. J. Howell[52], Y. M. Hu[10], E. A. Huerta[108], D. Huet[24], B. Hughey[103], S. Husa[86], S. H. Huttner[36], T. Huynh-Dinh[7], N. Indik[10], D. R. Ingram[37], R. Inta[72], H. N. Isa[36], J.-M. Isac[60], M. Isi[1], T. Isogai[12], B. R. Iyer[17], K. Izumi[37], T. Jacqmin[60], K. Jani[44], P. Jaranowski[109], S. Jawahar[110], F. Jiménez-Forteza[86], W. W. Johnson[2], D. I. Jones[111], R. Jones[36], R. J. G. Jonker[11], L. Ju[52], J. Junker[10], C. V. Kalaghatgi[94], V. Kalogera[85], S. Kandhasamy[73], G. Kang[79], J. B. Kanner[1], S. Karki[59], K. S. Karvinen[10], M. Kasprzack[2], E. Katsavounidis[12], W. Katzman[7], S. Kaufer[19], T. Kaur[52], K. Kawabe[37], F. Kéfélian[54], D. Keitel[86], D. B. Kelley[35], R. Kennedy[90], J. S. Key[112],

F. Y. Khalili[49], I. Khan[14], S. Khan[94], Z. Khan[89], E. A. Khazanov[113], N. Kijbunchoo[37], Chunglee Kim[114], J. C. Kim[115], Whansun Kim[116], W. Kim[70], Y.-M. Kim[114,117], S. J. Kimbrell[44], E. J. King[70], P. J. King[37], R. Kirchhoff[10], J. S. Kissel[37], B. Klein[85], L. Kleybolte[27], S. Klimenko[6], P. Koch[10], S. M. Koehlenbeck[10], S. Koley[11], V. Kondrashov[1], A. Kontos[12], M. Korobko[27], W. Z. Korth[1], I. Kowalska[62], D. B. Kozak[1], C. Krämer[10], V. Kringel[10], B. Krishnan[10], A. Królak[118,119], G. Kuehn[10], P. Kumar[97], R. Kumar[89], L. Kuo[75], A. Kutynia[118], B. D. Lackey[29,35], M. Landry[37], R. N. Lang[18], J. Lange[107], B. Lantz[40], R. K. Lanza[12], A. Lartaux-Vollard[24], P. D. Lasky[120], M. Laxen[7], A. Lazzarini[1], C. Lazzaro[42], P. Leaci[28,81], S. Leavey[36], E. O. Lebigot[30], C. H. Lee[117], H. K. Lee[121], H. M. Lee[114], K. Lee[36], J. Lehmann[10], A. Lenon[31], M. Leonardi[92,93], J. R. Leong[10], N. Leroy[24], N. Letendre[8], Y. Levin[120], T. G. F. Li[122], A. Libson[12], T. B. Littenberg[123], J. Liu[52], N. A. Lockerbie[110], A. L. Lombardi[44], L. T. London[94], J. E. Lord[35], M. Lorenzini[14,15], V. Loriette[124], M. Lormand[7], G. Losurdo[21], J. D. Lough[10,19], C. O. Lousto[107], G. Lovelace[23], H. Lück[10,19], A. P. Lundgren[10], R. Lynch[12], Y. Ma[51], S. Macfoy[50], B. Machenschalk[10], M. MacInnis[12], D. M. Macleod[2], F. Magaña-Sandoval[35], E. Majorana[28], I. Maksimovic[124], V. Malvezzi[15,26], N. Man[54], V. Mandic[125], V. Mangano[36], G. L. Mansell[22], M. Manske[18], M. Mantovani[34], F. Marchesoni[33,126], F. Marion[8], S. Márka[39], Z. Márka[39], A. S. Markosyan[40], E. Maros[1], F. Martelli[57,58], L. Martellini[54], I. W. Martin[36], D. V. Martynov[12], K. Mason[12], A. Masserot[8], T. J. Massinger[1], M. Masso-Reid[36], S. Mastrogiovanni[28,81], F. Matichard[1,12], L. Matone[39], N. Mavalvala[12], N. Mazumder[56], R. McCarthy[37], D. E. McClelland[22], S. McCormick[7], C. McGrath[18], S. C. McGuire[127], G. McIntyre[1], J. McIver[1], D. J. McManus[22], T. McRae[22], S. T. McWilliams[31], D. Meacher[54,74], G. D. Meadors[10,29], J. Meidam[11], A. Melatos[128], G. Mendell[37], D. Mendoza-Gandara[10], R. A. Mercer[18], E. L. Merilh[37], M. Merzougui[54], S. Meshkov[1], C. Messenger[36], C. Messick[74], R. Metzdorff[60], P. M. Meyers[125], F. Mezzani[28,81], H. Miao[45], C. Michel[65], H. Middleton[45], E. E. Mikhailov[129], L. Milano[5,67], A. L. Miller[6,28,81], A. Miller[85], B. B. Miller[85], J. Miller[12], M. Millhouse[84], Y. Minenkov[15], J. Ming[29], S. Mirshekari[130], C. Mishra[17], S. Mitra[16], V. P. Mitrofanov[49], G. Mitselmakher[6], R. Mittleman[12], A. Moggi[21], M. Mohan[34], S. R. P. Mohapatra[12], M. Montani[57,58], B. C. Moore[95], C. J. Moore[80], D. Moraru[37], G. Moreno[37], S. R. Morriss[87], B. Mours[8], C. M. Mow-Lowry[45], G. Mueller[6], A. W. Muir[94], Arunava Mukherjee[17], D. Mukherjee[18], S. Mukherjee[87], N. Mukund[16], A. Mullavey[7], J. Munch[70], E. A. M. Muniz[23], P. G. Murray[36], A. Mytidis[6], K. Napier[44], I. Nardecchia[15,26], L. Naticchioni[28,81], G. Nelemans[11,53], T. J. N. Nelson[7], M. Neri[46,47], M. Nery[10], A. Neunzert[106], J. M. Newport[3], G. Newton[36], T. T. Nguyen[22], A. B. Nielsen[10], S. Nissanke[11,53], A. Nitz[10], A. Noack[10], F. Nocera[34], D. Nolting[7], M. E. N. Normandin[87], L. K. Nuttall[35], J. Oberling[37], E. Ochsner[18], E. Oelker[12], G. H. Ogin[131], J. J. Oh[116], S. H. Oh[116], F. Ohme[10,94], M. Oliver[86], P. Oppermann[10], Richard J. Oram[7], B. O'Reilly[7], R. O'Shaughnessy[107], D. J. Ottaway[70], H. Overmier[7], B. J. Owen[72], A. E. Pace[74], J. Page[123], A. Pai[101], S. A. Pai[48], J. R. Palamos[59], O. Palashov[113], C. Palomba[28], A. Pal-Singh[27], H. Pan[75], C. Pankow[85], F. Pannarale[94], B. C. Pant[48], F. Paoletti[21,34], A. Paoli[34], M. A. Papa[10,18,29], H. R. Paris[40], W. Parker[7], D. Pascucci[36], A. Pasqualetti[34], R. Passaquieti[20,21], D. Passuello[21], B. Patricelli[20,21], B. L. Pearlstone[36], M. Pedraza[1], R. Pedurand[65,132], L. Pekowsky[35], A. Pele[7], S. Penn[133], C. J. Perez[37], A. Perreca[1], L. M. Perri[85], H. P. Pfeiffer[97], M. Phelps[36], O. J. Piccinni[28,81], M. Pichot[54], F. Piergiovanni[57,58], V. Pierro[9], G. Pillant[34], L. Pinard[65], I. M. Pinto[9], M. Pitkin[36], M. Poe[18], R. Poggiani[20,21], P. Popolizio[34], A. Post[10], J. Powell[36], J. Prasad[16], J. W. W. Pratt[103], V. Predoi[94], T. Prestegard[18,125], M. Prijatelj[10,34], M. Principe[9], S. Privitera[29], R. Prix[10], G. A. Prodi[92,93], L. G. Prokhorov[49], O. Puncken[10], M. Punturo[33], P. Puppo[28], M. Pürrer[29], H. Qi[18], J. Qin[52], S. Qiu[120], V. Quetschke[87], E. A. Quintero[1], R. Quitzow-James[59], F. J. Raab[37], D. S. Rabeling[22], H. Radkins[37], P. Raffai[98], S. Raja[48], C. Rajan[48], M. Rakhmanov[87], P. Rapagnani[28,81], V. Raymond[29], M. Razzano[20,21], V. Re[26], J. Read[23], T. Regimbau[54], L. Rei[47], S. Reid[50], D. H. Reitze[1,6], H. Rew[129], S. D. Reyes[35], E. Rhoades[103], F. Ricci[28,81], K. Riles[106], M. Rizzo[107], N. A. Robertson[1,36], R. Robie[36], F. Robinet[24], A. Rocchi[15], L. Rolland[8], J. G. Rollins[1], V. J. Roma[59], R. Romano[4,5], J. H. Romie[7], D. Rosińska[43,134], S. Rowan[36], A. Rüdiger[10], P. Ruggi[34], K. Ryan[37], S. Sachdev[1], T. Sadecki[37], L. Sadeghian[18], M. Sakellariadou[135], L. Salconi[34], M. Saleem[101], F. Salemi[10], A. Samajdar[136], L. Sammut[120], L. M. Sampson[85], E. J. Sanchez[1], V. Sandberg[37], J. R. Sanders[35], B. Sassolas[65], B. S. Sathyaprakash[74,94], P. R. Saulson[35], O. Sauter[106], R. L. Savage[37], A. Sawadsky[19], P. Schale[59], J. Scheuer[85], E. Schmidt[103], J. Schmidt[10], P. Schmidt[1,51], R. Schnabel[27], R. M. S. Schofield[59], A. Schönbeck[27], E. Schreiber[10], D. Schuette[10,19], B. F. Schutz[29,94], S. G. Schwalbe[103], J. Scott[36], S. M. Scott[22], D. Sellers[7], A. S. Sengupta[137], D. Sentenac[34], V. Sequino[15,26], A. Sergeev[113], Y. Setyawati[11,53], D. A. Shaddock[22], T. J. Shaffer[37], M. S. Shahriar[85], B. Shapiro[40], P. Shawhan[64], A. Sheperd[18], D. H. Shoemaker[12], D. M. Shoemaker[44], K. Siellez[44], X. Siemens[18], M. Sieniawska[43], D. Sigg[37], A. D. Silva[13], A. Singer[1], L. P. Singer[68], A. Singh[10,19,29], R. Singh[2], A. Singhal[14], A. M. Sintes[86], B. J. J. Slagmolen[22], B. Smith[7], J. R. Smith[23], R. J. E. Smith[1], E. J. Son[116], B. Sorazu[36], F. Sorrentino[47], T. Souradeep[16], A. P. Spencer[36], A. K. Srivastava[89], A. Staley[39], M. Steinke[10], J. Steinlechner[36], S. Steinlechner[27,36], D. Steinmeyer[10,19], B. C. Stephens[18], S. P. Stevenson[45], R. Stone[87], K. A. Strain[36], N. Straniero[65], G. Stratta[57,58], S. E. Strigin[49], R. Sturani[130], A. L. Stuver[7], T. Z. Summerscales[138], L. Sun[128], S. Sunil[89], P. J. Sutton[94], B. L. Swinkels[34], M. J. Szczepańczyk[103], M. Tacca[30], D. Talukder[59], D. B. Tanner[6], M. Tápai[102], A. Taracchini[29], R. Taylor[1], T. Theeg[10], E. G. Thomas[45], M. Thomas[7], P. Thomas[37], K. A. Thorne[7], E. Thrane[120], T. Tippens[44], S. Tiwari[14,93], V. Tiwari[94], K. V. Tokmakov[110], K. Toland[36], C. Tomlinson[90], M. Tonelli[20,21], Z. Tornasi[36], C. I. Torrie[1], D. Töyrä[45], F. Travasso[32,33], G. Traylor[7], D. Trifirò[73], J. Trinastic[6], M. C. Tringali[92,93], L. Trozzo[21,139], M. Tse[12], R. Tso[1], M. Turconi[54], D. Tuyenbayev[87], D. Ugolini[140], C. S. Unnikrishnan[104], A. L. Urban[1], S. A. Usman[94], H. Vahlbruch[19], G. Vajente[1], G. Valdes[87], N. van Bakel[11], M. van Beuzekom[11], J. F. J. van den Brand[11,63], C. Van Den Broeck[11], D. C. Vander-Hyde[35], L. van der Schaaf[11], J. V. van Heijningen[11], A. A. van Veggel[36], M. Vardaro[41,42], V. Varma[51], S. Vass[1], M. Vasúth[38], A. Vecchio[45], G. Vedovato[42], J. Veitch[45], P. J. Veitch[70], K. Venkateswara[141], G. Venugopalan[1], D. Verkindt[8], F. Vetrano[57,58], A. Viceré[57,58], A. D. Viets[18], S. Vinciguerra[45], D. J. Vine[50],

J.-Y. Vinet[54], S. Vitale[12], T. Vo[35], H. Vocca[32,33], C. Vorvick[37], D. V. Voss[6], W. D. Vousden[45], S. P. Vyatchanin[49], A. R. Wade[1], L. E. Wade[78], M. Wade[78], M. Walker[2], L. Wallace[1], S. Walsh[10,29], G. Wang[14,58], H. Wang[45], M. Wang[45], Y. Wang[52], R. L. Ward[22], J. Warner[37], M. Was[8], J. Watchi[82], B. Weaver[37], L.-W. Wei[54], M. Weinert[10], A. J. Weinstein[1], R. Weiss[12], L. Wen[52], P. Weßels[10], T. Westphal[10], K. Wette[10], J. T. Whelan[107], B. F. Whiting[6], C. Whittle[120], D. Williams[36], R. D. Williams[1], A. R. Williamson[94], J. L. Willis[142], B. Willke[10,19], M. H. Wimmer[10,19], W. Winkler[10], C. C. Wipf[1], H. Wittel[10,19], G. Woan[36], J. Woehler[10], J. Worden[37], J. L. Wright[36], D. S. Wu[10], G. Wu[7], W. Yam[12], H. Yamamoto[1], C. C. Yancey[64], M. J. Yap[22], Hang Yu[12], Haocun Yu[12], M. Yvert[8], A. Zadrożny[118], L. Zangrando[42], M. Zanolin[103], J.-P. Zendri[42], M. Zevin[85], L. Zhang[1], M. Zhang[129], T. Zhang[36], Y. Zhang[107], C. Zhao[52], M. Zhou[85], Z. Zhou[85], S. J. Zhu[29,10], X. J. Zhu[52], M. E. Zucker[1,12], J. Zweizig[1]

(LIGO Scientific Collaboration and Virgo Collaboration),

S. Buchner[143,144], I. Cognard[145,146], A. Corongiu[147], P. C. C. Freire[148], L. Guillemot[145,146], G. B. Hobbs[149], M. Kerr[149], A. G. Lyne[150], A. Possenti[147], A. Ridolfi[148], R. M. Shannon[151,152], B. W. Stappers[150], and P. Weltevrede[150]

[1] LIGO, California Institute of Technology, Pasadena, CA 91125, USA
[2] Louisiana State University, Baton Rouge, LA 70803, USA
[3] American University, Washington, DC 20016, USA
[4] Università di Salerno, Fisciano, I-84084 Salerno, Italy
[5] INFN, Sezione di Napoli, Complesso Universitario di Monte S.Angelo, I-80126 Napoli, Italy
[6] University of Florida, Gainesville, FL 32611, USA
[7] LIGO Livingston Observatory, Livingston, LA 70754, USA
[8] Laboratoire d'Annecy-le-Vieux de Physique des Particules (LAPP), Université Savoie Mont Blanc, CNRS/IN2P3, F-74941 Annecy-le-Vieux, France
[9] University of Sannio at Benevento, I-82100 Benevento, Italy and INFN, Sezione di Napoli, I-80100 Napoli, Italy
[10] Albert-Einstein-Institut, Max-Planck-Institut für Gravitationsphysik, D-30167 Hannover, Germany
[11] Nikhef, Science Park, 1098 XG Amsterdam, The Netherlands
[12] LIGO, Massachusetts Institute of Technology, Cambridge, MA 02139, USA
[13] Instituto Nacional de Pesquisas Espaciais, 12227-010 São José dos Campos, São Paulo, Brazil
[14] INFN, Gran Sasso Science Institute, I-67100 L'Aquila, Italy
[15] INFN, Sezione di Roma Tor Vergata, I-00133 Roma, Italy
[16] Inter-University Centre for Astronomy and Astrophysics, Pune 411007, India
[17] International Centre for Theoretical Sciences, Tata Institute of Fundamental Research, Bengaluru 560089, India
[18] University of Wisconsin-Milwaukee, Milwaukee, WI 53201, USA
[19] Leibniz Universität Hannover, D-30167 Hannover, Germany
[20] Università di Pisa, I-56127 Pisa, Italy
[21] INFN, Sezione di Pisa, I-56127 Pisa, Italy
[22] Australian National University, Canberra, Australian Capital Territory 0200, Australia
[23] California State University Fullerton, Fullerton, CA 92831, USA
[24] LAL, Univ. Paris-Sud, CNRS/IN2P3, Université Paris-Saclay, F-91898 Orsay, France
[25] Chennai Mathematical Institute, Chennai 603103, India
[26] Università di Roma Tor Vergata, I-00133 Roma, Italy
[27] Universität Hamburg, D-22761 Hamburg, Germany
[28] INFN, Sezione di Roma, I-00185 Roma, Italy
[29] Albert-Einstein-Institut, Max-Planck-Institut für Gravitationsphysik, D-14476 Potsdam-Golm, Germany
[30] APC, AstroParticule et Cosmologie, Université Paris Diderot, CNRS/IN2P3, CEA/Irfu, Observatoire de Paris, Sorbonne Paris Cité, F-75205 Paris Cedex 13, France
[31] West Virginia University, Morgantown, WV 26506, USA
[32] Università di Perugia, I-06123 Perugia, Italy
[33] INFN, Sezione di Perugia, I-06123 Perugia, Italy
[34] European Gravitational Observatory (EGO), I-56021 Cascina, Pisa, Italy
[35] Syracuse University, Syracuse, NY 13244, USA
[36] SUPA, University of Glasgow, Glasgow G12 8QQ, UK
[37] LIGO Hanford Observatory, Richland, WA 99352, USA
[38] Wigner RCP, RMKI, H-1121 Budapest, Konkoly Thege Miklós út 29–33, Hungary
[39] Columbia University, New York, NY 10027, USA
[40] Stanford University, Stanford, CA 94305, USA
[41] Università di Padova, Dipartimento di Fisica e Astronomia, I-35131 Padova, Italy
[42] INFN, Sezione di Padova, I-35131 Padova, Italy
[43] Nicolaus Copernicus Astronomical Center, Polish Academy of Sciences, 00-716, Warsaw, Poland
[44] Center for Relativistic Astrophysics and School of Physics, Georgia Institute of Technology, Atlanta, GA 30332, USA
[45] University of Birmingham, Birmingham B15 2TT, UK
[46] Università degli Studi di Genova, I-16146 Genova, Italy
[47] INFN, Sezione di Genova, I-16146 Genova, Italy
[48] RRCAT, Indore MP 452013, India
[49] Faculty of Physics, Lomonosov Moscow State University, Moscow 119991, Russia
[50] SUPA, University of the West of Scotland, Paisley PA1 2BE, UK
[51] Caltech CaRT, Pasadena, CA 91125, USA
[52] University of Western Australia, Crawley, Western Australia 6009, Australia
[53] Department of Astrophysics/IMAPP, Radboud University Nijmegen, P.O. Box 9010, 6500 GL Nijmegen, The Netherlands
[54] Artemis, Université Côte d'Azur, CNRS, Observatoire Côte d'Azur, CS 34229, F-06304 Nice Cedex 4, France
[55] Institut de Physique de Rennes, CNRS, Université de Rennes 1, F-35042 Rennes, France
[56] Washington State University, Pullman, WA 99164, USA
[57] Università degli Studi di Urbino "Carlo Bo", I-61029 Urbino, Italy
[58] INFN, Sezione di Firenze, I-50019 Sesto Fiorentino, Firenze, Italy
[59] University of Oregon, Eugene, OR 97403, USA
[60] Laboratoire Kastler Brossel, UPMC-Sorbonne Universités, CNRS, ENS-PSL Research University, Collège de France, F-75005 Paris, France
[61] Carleton College, Northfield, MN 55057, USA

[62] Astronomical Observatory Warsaw University, 00-478 Warsaw, Poland
[63] VU University Amsterdam, 1081 HV Amsterdam, The Netherlands
[64] University of Maryland, College Park, MD 20742, USA
[65] Laboratoire des Matériaux Avancés (LMA), CNRS/IN2P3, F-69622 Villeurbanne, France
[66] Université Claude Bernard Lyon 1, F-69622 Villeurbanne, France
[67] Università di Napoli "Federico II", Complesso Universitario di Monte S.Angelo, I-80126 Napoli, Italy
[68] NASA/Goddard Space Flight Center, Greenbelt, MD 20771, USA
[69] RESCEU, University of Tokyo, Tokyo, 113-0033, Japan
[70] University of Adelaide, Adelaide, South Australia 5005, Australia
[71] Tsinghua University, Beijing 100084, China
[72] Texas Tech University, Lubbock, TX 79409, USA
[73] The University of Mississippi, University, MS 38677, USA
[74] The Pennsylvania State University, University Park, PA 16802, USA
[75] National Tsing Hua University, Hsinchu City, 30013 Taiwan, Republic of China
[76] Charles Sturt University, Wagga Wagga, New South Wales 2678, Australia
[77] University of Chicago, Chicago, IL 60637, USA
[78] Kenyon College, Gambier, OH 43022, USA
[79] Korea Institute of Science and Technology Information, Daejeon 305-806, Korea
[80] University of Cambridge, Cambridge CB2 1TN, UK
[81] Università di Roma "La Sapienza", I-00185 Roma, Italy
[82] University of Brussels, Brussels 1050, Belgium
[83] Sonoma State University, Rohnert Park, CA 94928, USA
[84] Montana State University, Bozeman, MT 59717, USA
[85] Center for Interdisciplinary Exploration & Research in Astrophysics (CIERA), Northwestern University, Evanston, IL 60208, USA
[86] Universitat de les Illes Balears, IAC3—IEEC, E-07122 Palma de Mallorca, Spain
[87] The University of Texas Rio Grande Valley, Brownsville, TX 78520, USA
[88] Bellevue College, Bellevue, WA 98007, USA
[89] Institute for Plasma Research, Bhat, Gandhinagar 382428, India
[90] The University of Sheffield, Sheffield S10 2TN, UK
[91] California State University, Los Angeles, 5154 State University Dr, Los Angeles, CA 90032, USA
[92] Università di Trento, Dipartimento di Fisica, I-38123 Povo, Trento, Italy
[93] INFN, Trento Institute for Fundamental Physics and Applications, I-38123 Povo, Trento, Italy
[94] Cardiff University, Cardiff CF24 3AA, UK
[95] Montclair State University, Montclair, NJ 07043, USA
[96] National Astronomical Observatory of Japan, 2-21-1 Osawa, Mitaka, Tokyo 181-8588, Japan
[97] Canadian Institute for Theoretical Astrophysics, University of Toronto, Toronto, Ontario M5S 3H8, Canada
[98] MTA Eötvös University, "Lendulet" Astrophysics Research Group, Budapest 1117, Hungary
[99] School of Mathematics, University of Edinburgh, Edinburgh EH9 3FD, UK
[100] University and Institute of Advanced Research, Gandhinagar, Gujarat 382007, India
[101] IISER-TVM, CET Campus, Trivandrum Kerala 695016, India
[102] University of Szeged, Dóm tér 9, Szeged 6720, Hungary
[103] Embry-Riddle Aeronautical University, Prescott, AZ 86301, USA
[104] Tata Institute of Fundamental Research, Mumbai 400005, India
[105] INAF, Osservatorio Astronomico di Capodimonte, I-80131, Napoli, Italy
[106] University of Michigan, Ann Arbor, MI 48109, USA
[107] Rochester Institute of Technology, Rochester, NY 14623, USA
[108] NCSA, University of Illinois at Urbana-Champaign, Urbana, IL 61801, USA
[109] University of Białystok, 15-424 Białystok, Poland
[110] SUPA, University of Strathclyde, Glasgow G1 1XQ, UK
[111] University of Southampton, Southampton SO17 1BJ, UK
[112] University of Washington Bothell, 18115 Campus Way NE, Bothell, WA 98011, USA
[113] Institute of Applied Physics, Nizhny Novgorod, 603950, Russia
[114] Seoul National University, Seoul 151-742, Korea
[115] Inje University Gimhae, 621-749 South Gyeongsang, Korea
[116] National Institute for Mathematical Sciences, Daejeon 305-390, Korea
[117] Pusan National University, Busan 609-735, Korea
[118] NCBJ, 05-400 Świerk-Otwock, Poland
[119] Institute of Mathematics, Polish Academy of Sciences, 00656 Warsaw, Poland
[120] Monash University, Victoria 3800, Australia
[121] Hanyang University, Seoul 133-791, Korea
[122] The Chinese University of Hong Kong, Shatin, NT, Hong Kong
[123] University of Alabama in Huntsville, Huntsville, AL 35899, USA
[124] ESPCI, CNRS, F-75005 Paris, France
[125] University of Minnesota, Minneapolis, MN 55455, USA
[126] Università di Camerino, Dipartimento di Fisica, I-62032 Camerino, Italy
[127] Southern University and A&M College, Baton Rouge, LA 70813, USA
[128] The University of Melbourne, Parkville, Victoria 3010, Australia
[129] College of William and Mary, Williamsburg, VA 23187, USA
[130] Instituto de Física Teórica, University Estadual Paulista/ICTP South American Institute for Fundamental Research, São Paulo SP 01140-070, Brazil
[131] Whitman College, 345 Boyer Avenue, Walla Walla, WA 99362 USA
[132] Université de Lyon, F-69361 Lyon, France
[133] Hobart and William Smith Colleges, Geneva, NY 14456, USA
[134] Janusz Gil Institute of Astronomy, University of Zielona Góra, 65-265 Zielona Góra, Poland
[135] King's College London, University of London, London WC2R 2LS, UK
[136] IISER-Kolkata, Mohanpur, West Bengal 741252, India
[137] Indian Institute of Technology, Gandhinagar Ahmedabad Gujarat 382424, India

[138] Andrews University, Berrien Springs, MI 49104, USA
[139] Università di Siena, I-53100 Siena, Italy
[140] Trinity University, San Antonio, TX 78212, USA
[141] University of Washington, Seattle, WA 98195, USA
[142] Abilene Christian University, Abilene, TX 79699, USA
[143] Square Kilometer Array South Africa, The Park, Park Road, Pinelands, Cape Town 7405, South Africa
[144] Hartebeesthoek Radio Astronomy Observatory, PO Box 443, Krugersdorp, 1740, South Africa
[145] Laboratoire de Physique et Chimie de l'Environnement et de l'Espace, LPC2E, CNRS-Université d'Orléans, F-45071 Orléans, France
[146] Station de Radioastronomie de Nançay, Observatoire de Paris, CNRS/INSU, F-18330 Nançay, France
[147] INAF—Osservatorio Astronomico di Cagliari, via della Scienza 5, 09047 Selargius, Italy
[148] Max-Planck-Institut für Radioastronomie MPIfR, Auf dem Hügel 69, D-53121 Bonn, Germany
[149] CSIRO Astronomy and Space Science, Australia Telescope National Facility, Box 76 Epping, NSW, 1710, Australia
[150] Jodrell Bank Centre for Astrophysics, School of Physics and Astronomy, University of Manchester, Manchester M13 9PL, UK
[151] CSIRO Astronomy and Space Science, Australia Telescope National Facility, Box 76 Epping, NSW, 1710, Australia
[152] International Centre for Radio Astronomy Research, Curtin University, Bentley, WA 6102, Australia

Abstract

We present the result of searches for gravitational waves from 200 pulsars using data from the first observing run of the Advanced LIGO detectors. We find no significant evidence for a gravitational-wave signal from any of these pulsars, but we are able to set the most constraining upper limits yet on their gravitational-wave amplitudes and ellipticities. For eight of these pulsars, our upper limits give bounds that are improvements over the indirect spin-down limit values. For another 32, we are within a factor of 10 of the spin-down limit, and it is likely that some of these will be reachable in future runs of the advanced detector. Taken as a whole, these new results improve on previous limits by more than a factor of two.

1. Introduction

The recent observations of gravitational waves from the inspiral and merger of binary black holes herald the era of gravitational-wave astronomy (Abbott et al. 2016b, 2016c). Such cataclysmic, transient, and extragalatic events are not however the only potential sources of observable gravitational waves. Galactic neutron stars offer a more local, and continuous, quasi-monochromatic source of gravitational radiation. Although intrinsically far weaker than the transient sources that have been observed, their continuous nature allows their signals to be found buried deep in the noise by coherently integrating over the long observing runs of the gravitational-wave observatories.

The subset of known pulsars, identified through electromagnetic observations, provides an important possible source of continuous gravitational waves. They are often timed with exquisite precision, allowing their rotational phase evolution, sky location and, if required, binary orbital parameters to be determined very accurately. In turn, these timings allow us to carry out fully phase-coherent and computationally cheap gravitational-wave searches over the length of our observation runs. A selection of known pulsars have already been targeted using data from the initial LIGO, Virgo, and GEO 600 detectors (summarized in Aasi et al. 2014), setting upper limits on their signal amplitudes, though without any detections.

An important milestone is passed when this upper limit falls below the so-called spin-down limit on gravitational strain for the targeted pulsar. This spin-down limit is determined by equating the power radiated through gravitational-wave emission to the pulsar's observed spin-down luminosity (attributed to its loss in rotational kinetic energy), i.e., as would be the case if it were a *gravitar* (Palomba 2005;

Knispel & Allen 2008), and determining the equivalent strain expected at Earth.[154] It can be calculated (see, e.g., Aasi et al. 2014) using

$$h_0^{\rm sd} = \left(\frac{5}{2} \frac{G I_{zz} |\dot{f}_{\rm rot}|}{c^3 d^2 f_{\rm rot}} \right)^{1/2}, \qquad (1)$$

where $f_{\rm rot}$ and $\dot{f}_{\rm rot}$ are the pulsar's frequency and first frequency derivative, I_{zz} is the principal moment of inertia (for which we generally assume a canonical value of $10^{38}\,{\rm kg\,m^2}$), and d is the pulsar's distance. In previous searches, this limit has been surpassed (i.e., a smaller limit on the strain amplitude has been obtained) for two pulsars: PSR J0534+2200 (the Crab pulsar; Abbott et al. 2008) and PSR J0835−4510 (the Vela pulsar; Abadie et al. 2011).

In this paper, we provide results from a search for gravitational waves from 200 known pulsars using data from the first observing run (O1) of Advanced LIGO (aLIGO). For the LIGO Hanford Observatory (H1) and LIGO Livingston Observatory (L1), we used data starting on 2015 September 11 at 01:25:03 UTC and 18:29:03 UTC, respectively, and finishing on 2016 January 19 at 17:07:59 UTC at both sites. With duty factors of 60% and 51% for H1 and L1, this run provided 78 days and 66 days of data respectively for analysis. The estimated sensitivity of this search as a function

---

[153] Deceased, 2016 March.

[154] This is known to be a naïve limit. For several young pulsars where the braking index (see Section 4) is measured (Lyne et al. 2015; Archibald et al. 2016), we know that it is not consistent with pure gravitational-wave emission, and other energy-loss mechanisms can be dominant. Effects of this on spin-down limit calculations are discussed in Palomba (2000). Figures 9 and 10 of Abdo et al. (2013) also show that for pulsars observed as *Fermi* gamma-ray sources, a not insignificant proportion of their spin-down luminosity is emitted through gamma-rays.

of source frequency is shown in Figure 1.[155] We see that, even with its comparatively short observation time, the O1 data provide a significant sensitivity improvement over the previous runs, particularly at lower frequencies.

1.1. The Signal

We model the source as a rigidly rotating triaxial star, generating a strain signal at the detector of (e.g., Jaranowski et al. 1998)

$$h(t) = h_0 \left[\frac{1}{2} F_+^D(t, \alpha, \delta, \psi)(1 + \cos^2 \iota) \cos \phi(t) \right.$$
$$\left. + F_\times^D(t, \alpha, \delta, \psi) \cos \iota \sin \phi(t) \right], \qquad (2)$$

where h_0 is the gravitational-wave strain amplitude, and F_+^D and $F_\times^D$ are the antenna responses of observatory D to the "+" and "×" polarizations. These are dependent on the source sky position (right ascension α and declination δ) and polarization angle ψ. ι is the inclination of the star's rotation axis to the line of sight, and $\phi(t)$ represents the evolution of the sinusoidal signal phase with time.

This phase evolution is usefully represented as a Taylor expansion, so that

$$\phi(t) = \phi_0 + 2\pi \sum_{j=0}^N \frac{f_0^{(j)}}{(j+1)!} (t - T_0 + \delta t(t))^{(j+1)}, \qquad (3)$$

where ϕ_0 is the initial gravitational-wave phase at time epoch T_0, and $f_0^{(j)}$ is the jth time derivative of the gravitational-wave frequency defined at T_0. $\delta t(t)$ is the time delay from the observatory to the solar system barycenter, and can also include binary system barycentering corrections to put the observatory and source in inertial frames. For the majority of pulsars, expansions to $N = 1$ or 2 are all that are required, but for some young sources, with significant timing noise, expansions to higher orders may be used. For the case of a source rotating around a principal axis of inertia and producing emission from the $l = m = 2$ (spherical harmonic) mass quadrupole mode (e.g., a rigidly rotating star with a triaxial moment of inertia ellipsoid), the gravitational-wave frequencies and frequency derivatives are all twice their rotational values, e.g., $f = 2f_{\rm rot}$.

2. Pulsar Selection

To reflect the improved sensitivity of LIGO during O1, we targeted pulsars with rotation frequencies, $f_{\rm rot}$, greater than about 10 Hz, but also included seven promising sources with large spin-down luminosities[156] with $f_{\rm rot}$ just below 10 Hz. The $l = m = 2$ quadrupolar emission frequencies of these targets are therefore greater than ~20 Hz and within the band of good sensitivity for the instruments. We did not impose an upper limit on target frequency.

We have obtained timings for 200 known pulsars in this band. Timing was performed using the 42 ft telescope and Lovell telescope at Jodrell Bank (UK), the 26 m telescope at Hartebeesthoek (South Africa), the Parkes radio telescope (Australia), the Nançay Decimetric Radio Telescope (France), the Arecibo Observatory (Puerto Rico) and the *Fermi* Large Area Telescope (LAT). Of these, 122 have been targeted in previous campaigns (Aasi et al. 2014), while 78 are new to this search.

For the vast majority of these, we have obtained timing solutions using pulse time-of-arrival (TOA) observations that spanned the O1 run. For those pulsars whose TOAs did not span O1, we still expect them to maintain very good coherence when extrapolated to the O1 time. The TEMPO[157] or TEMPO2 (Hobbs et al. 2006) pulsar timing codes were used to produce these solutions, which provide us with precise information on the parameters defining each pulsars phase evolution, including their sky location and any binary system orbital dynamics if applicable.[158]

2.1. High-value Targets

We identified 11 sources (Table 1) for which we could either improve upon, or closely approach, the spin-down limit based on Equation (1). These are all young pulsars at the lower end of our sensitive frequency band and include the Crab and Vela pulsars for which the spin-down limit had already been surpassed (Abbott et al. 2008; Abadie et al. 2011; Aasi et al. 2014).

3. Analyses

Following Aasi et al. (2014), we used three largely independent methods for carrying out the search for the 11 high-value targets: the time-domain-based *Bayesian* (Dupuis & Woan 2005) and $\mathcal{F}/\mathcal{G}$-*statistic* (Jaranowski & Królak 2010) methods, and the frequency-domain-based *5n*-vector method (Astone et al. 2010, 2012). For the other 189 targets only the *Bayesian* method was applied.

We refer the reader to Aasi et al. (2014) and references therein for more detailed descriptions of these methods. Generally, the methods were not modified for O1, although there have been some significant improvements to the *Bayesian* method, which are described in Appendix A.

In addition, the results from the 5n-vector method used an earlier data release, with a slightly different instrumental calibration (Abbott et al. 2016a), than that used for the two other methods. The calibrations applied differ, however, by less than 3% in amplitude and less than 3° in phase for all high-value sources.

For one high-value target, PSR J1302−6350, the *5n*-vector method was not used. This pulsar is in a binary system, which is not currently handled by this method. PSR J0205+6449 underwent a glitch on MJD 57345 (2015 November 19), causing the rotation frequency to increase by ~8.3 × 10⁻⁶ Hz. Because of the uncertain relation between the gravitational-wave and electromagnetic signal phases over a glitch, we analyzed both the pre-and-post-glitch periods independently and combined these incoherently to give the final result. To the best of our knowledge, none of our other sources glitched during the course of O1.

---

[155] The sensitivity is taken as $10.8\sqrt{S_n'}$, where S_n' is the harmonic mean of the observation-time-weighted one-sided power spectral densities, S_n/T, for H1 and L1 (see https://dcc.ligo.org/LIGO-G1600150/public and https://dcc.ligo.org/LIGO-G1600151/public, respectively). The factor of 10.8 gives the 95% credible upper limit on gravitational-wave strain amplitude averaged over orientation angles assuming Gaussian noise (Dupuis & Woan 2005).
[156] PSRs J0908−4913, J1418−6058, J1709−4429, J1826−1334, J1845−0743, J1853−0004, and J2129+1210A.

[157] http://tempo.sourceforge.net
[158] Of the 200 pulsars, 119 are in binary systems.
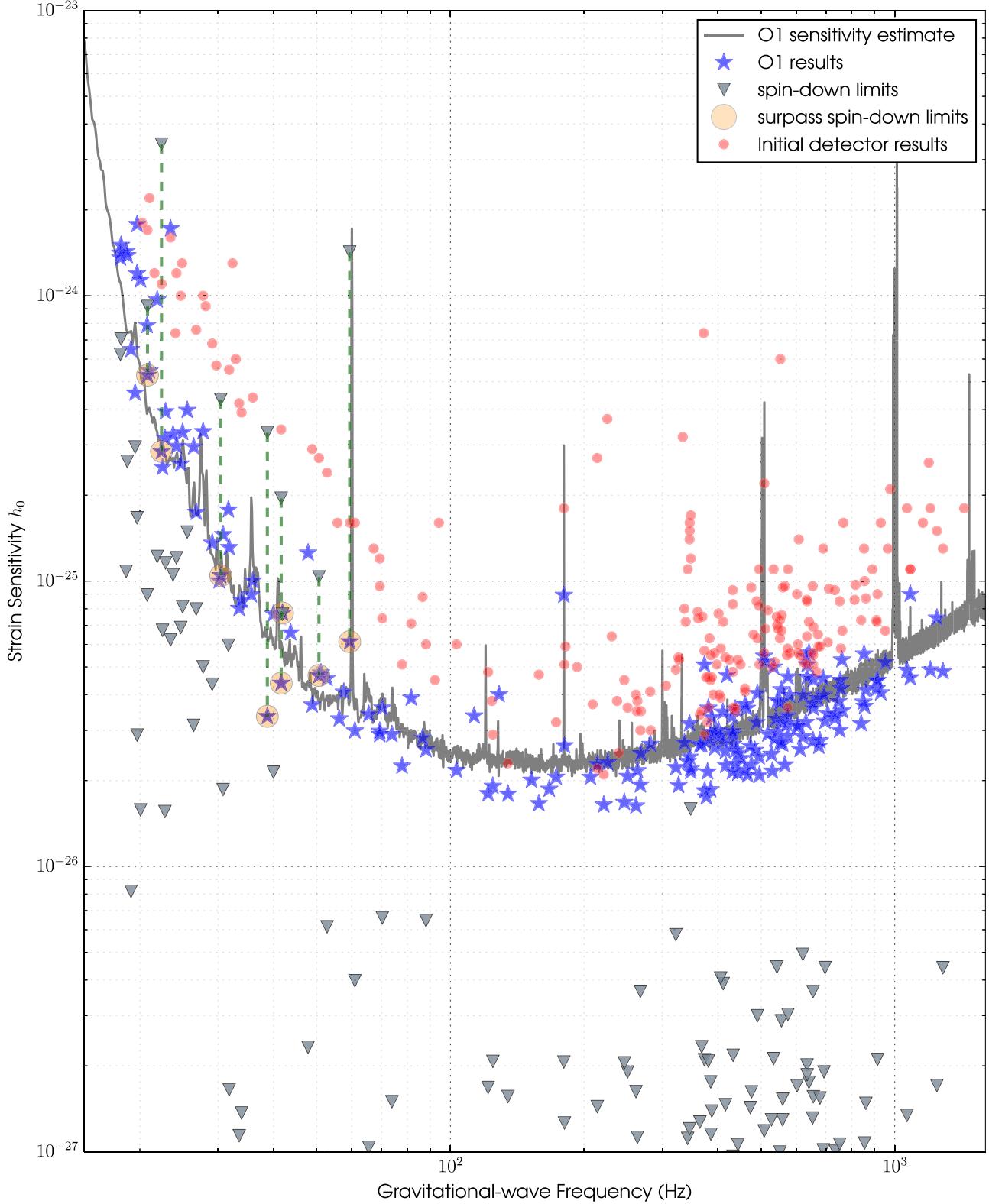
Figure 1. Stars show 95% credible upper limits on gravitational-wave amplitude, $h_0^{95\%}$, for 200 pulsars using data from the O1 run. ▼ give the spin-down limits for all pulsars (based on distance values taken from the ATNF pulsar catalog (Manchester et al. 2005), unless otherwise stated in Tables 1 and 4) and assuming the canonical moment of inertia. The upper limits shown within the shaded circles are those for which the spin-down limits (linked via the dashed vertical lines) are surpassed with our observations. The gray curve gives an estimate of the expected strain sensitivity for O1, combining representative amplitude spectral density measurements for both H1 and L1. This estimate is an angle-averaged value and for particular sources is representative only, while the broader range over all angles for such an estimate is shown, for example, in Figure 4 of Abbott et al. (2010). Previous initial detector run results (Aasi et al. 2014) for 195 pulsars are shown as red circles, with 122 of these sources corresponding to sources searched for in O1.

Table 1
The High-value Targets for Which the Spin-down Limit can be Improved Upon
or Closely Approached

PSR	f (Hz)	d (kpc)	$h_0^{\text{spin-down}}$
J0205+6449[a]	30.4	3.2	4.3×10^{-25}
J0534+2200 (Crab)	59.3	2.0	1.4×10^{-24}
J0835−4510 (Vela)	22.4	0.3	3.4×10^{-24}
J1302−6350[b]	41.9	2.3	7.7×10^{-26}
J1809−1917	24.2	3.7	1.2×10^{-25}
J1813−1246	41.6	2.5[c]	2.0×10^{-25}
J1826−1256	18.1	1.2[d]	7.1×10^{-25}
J1928+1746	29.1	8.1	4.4×10^{-26}
J1952+3252 (CTB 80)	50.6	3.0	1.0×10^{-25}
J2043+2740	20.8	1.1	9.2×10^{-25}
J2229+6114	38.7	3.0	3.3×10^{-25}

Notes. Unless otherwise stated, all distances are those from v1.54 of the ATNF Pulsar Catalog (Manchester et al. 2005).
[a] This pulsar was observed to glitch during O1 on MJD 57345.
[b] This pulsar is in a binary system and as such was not able to be searched for with the 5n-vector method.
[c] This distance is a lower limit on the distance from Marelli et al. (2014). It is slightly higher than the distance of 1.9 kpc used for calculations in Aasi et al. (2014).
[d] This distance is that taken from the lower distance range from Voisin et al. (2016; using values from Wang 2011).

The results from the *Bayesian* method incorporate uncertainties into the pulsars' phase evolutions. If the fits to pulsar TOAs from electromagnetic observations provided uncertainties on any fitted parameters, then these parameters were also included in the search space (in addition to the four main unknown signal parameters, h_0, ϕ_0, $\cos\iota$ and ψ, defined with Equations (2) and (3)). Prior probabilities for these additional parameters were defined as Gaussian distributions, using their best-fit values and associated errors as means and standard deviations (see, e.g., Abbott et al. 2010). Upper limits are produced from the posterior probability distributions on h_0 by marginalizing all other parameters over their prior ranges (see Appendix A.2) and calculating the h_0 value bounding (from zero) 95% of the probability (e.g., Equation (3.3) of Abbott et al. 2007).

Observations of pulsar-wind nebulae (PWNe) around several pulsars allow us to put prior constraints on their orientation angles ι and ψ, detailed in Appendix B. For these pulsars, any results given include both those based on the standard prior ranges for the orientation angles given in Equation (9), as well as those based on these restricted ranges.

4. Results

For all pulsars, we quote 95% credible/confidence upper limits on the gravitational-wave amplitude h_0 set using coherently combined data from both H1 and L1.[159] We use this value to also set limits on the mass quadrupole moment Q_{22} of the $l = m = 2$ mode of the star (Owen 2005) via

$$Q_{22} = h_0 \left(\frac{c^4 d}{16\pi^2 G f_{\text{rot}}^2} \right). \qquad (4)$$

---

[159] For the Bayesian results, these are credible limits bounded from zero, while for the frequentist results these are confidence limits.

In turn, this is related to the star's fiducial equatorial ellipticity ε through

$$\varepsilon = \frac{Q_{22}}{I_{zz}} \sqrt{\frac{8\pi}{15}}. \qquad (5)$$

To calculate ε, we use the canonical moment of inertia of $I_{zz} = 10^{38} \text{ kg m}^2$ (see, e.g., Chapter 6 of Condon & Ransom 2016). We also quote the ratio of our observed h_0 limits to the spin-down limits calculated using Equation (1). The distances used to calculate Q_{22} and ε are (unless otherwise stated in Tables 1 or 4) taken from v1.54 of the ATNF pulsar catalog (Manchester et al. 2005),[160] and in most cases are calculated from the observed dispersion measure (noting that distance uncertainties of 20% or more are not uncommon; see, e.g., Figure 12 of Cordes & Lazio 2002). For the spin-down limit calculation, we generally use values of $\dot{f}_{\text{rot}}$ provided from the electromagnetic-pulse-arrival-time fits used in our search. If, however, an intrinsic period derivative, i.e., a period derivative corrected for proper motion effects (Shklovskii 1969) or globular cluster accelerations, is given in the ATNF catalog, then that value is used. If an intrinsic period derivative is not given for a globular cluster pulsar, then the spin-down limit is instead based on an assumed characteristic spin-down age of $\tau = 10^9$ yr. The characteristic age (see, e.g., Chapter 6 of Condon & Ransom 2016) is defined as

$$\tau = -\frac{f_{\text{rot}}}{\dot{f}_{\text{rot}} (n - 1)}, \qquad (6)$$

where n is the braking index ($n = f_{\text{rot}} \ddot{f}_{\text{rot}} / \dot{f}_{\text{rot}}^2$), which has a value of $n = 3$ for purely magnetic dipole radiation, while we adopt the $n = 5$ case for purely gravitational radiation.

The calibration procedure for the aLIGO instruments and their amplitude uncertainties during the initial part of O1 are described in detail in Abbott et al. (2016a). After O1 was completed, the calibration was updated, and the maximum calibration uncertainties estimated over the whole run give a 1σ limit on the combined H1 and L1 amplitude uncertainties of $\lesssim 14\%$. This is the conservative level of uncertainty on the h_0 upper limits, and any quantities derived linearly from them, from the gravitational-wave observations alone.

The results for all targets, except the high-value targets discussed in Section 2.1, are shown in Table 4. For each pulsar, we produce two probability ratios, or odds (discussed in Appendix A.3): $\mathcal{O}_{\text{S/N}}$, Equation (11), comparing the probability that the data from both detectors contain a coherent signal matching our model to the probability that they both contain just (potentially non-stationary) Gaussian noise; and, $\mathcal{O}_{\text{S/I}}$, Equation (12), comparing the probability that the data from both detectors contain a coherent signal matching our model to the probability of the data containing combinations of independent signals or noise. The latter of these is an attempt to account for incoherent interference in the detectors (e.g., produced by instrumental line artifacts) that can mimic the effects of a signal. The distributions of these odds for all our sources can be seen in Figure 2.[161] We find that the largest ratio for $\mathcal{O}_{\text{S/I}}$ is 8 for PSR J1932+17. Although this is larger than

---

[161] For each source, a different prior volume was used, so directly comparing odds values between sources should be treated with caution.
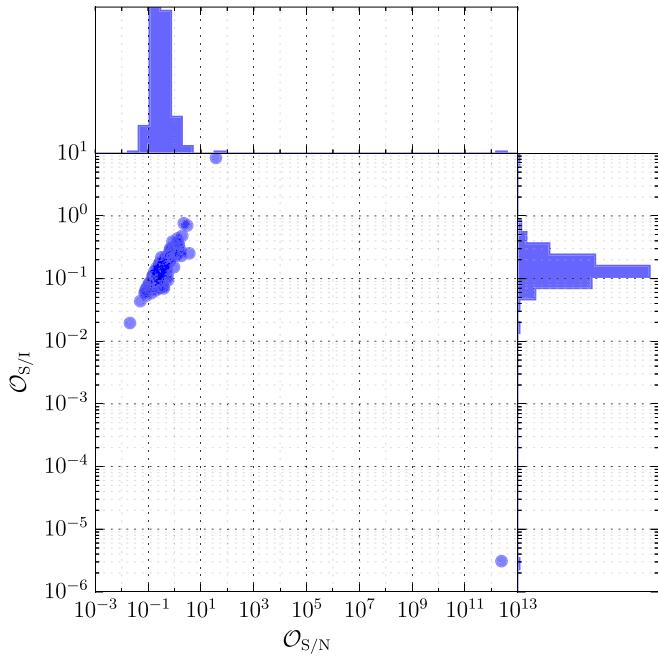
Figure 2. Distributions of the probability ratios $\mathcal{O}_{S/N}$ and $\mathcal{O}_{S/I}$ for the observed pulsars.

any other source and favors a coherent signal over the alternative incoherent-*or*-noise hypothesis by over a factor of eight, it is not yet strong enough evidence for a signal (e.g., in the interpretation scaling of Jeffreys 1998), especially considering the multiple searches that are performed. The largest $\mathcal{O}_{S/N}$ value is for PSR J1833−0827, with a value of 2.5×10^{12} in favor of the signal model. However, as is apparent from the $\mathcal{O}_{S/I}$ value of 3×10^{-6} and the posterior distributions of parameters, it is clear that the very large $\mathcal{O}_{S/N}$ comes from strong interference in the data, while there is no support for a coherent signal in both detectors.

The h_0 upper limits from this analysis (including those from the high-value targets) are shown in Figure 1. The figure also contains the upper limits obtained for the 195 pulsars targeted using data from the initial detector era (Aasi et al. 2014). We find that, on average, for pulsars that were both analyzed here and in previous runs, our new results have over two and a half times better sensitivity. The largest improvement is a factor of eight for PSR J0024−7204C at $f = 347.4$ Hz. For four pulsars, the new results are slightly less sensitive than the previous analyses, although in the worst case this is only by $\lesssim 10\%$.[162]

Figure 3 shows corresponding limits on the fiducial ellipticity ε and mass quadrupole moment Q_{22}. Figure 4 shows a histogram of the ratios between our upper limits and the spin-down limits.

The accelerations that pulsars experience in the cores of globular clusters can mask their true spin-down values. It is sometimes possible to determine these accelerations and correct for their effect on spin-down. As mentioned above, when such a correction is available, we have calculated the spin-down limits based on this corrected spin-down value. In cases where the correction is not available, we have instead assumed each pulsar has a characteristic age of $\tau = 10^9$ yr

and under the assumption of gravitational-radiation-dominated spin-down, calculated a naïve spin-down via Equation (6), which has then been used for the spin-down limit calculation. As proposed in Pitkin (2011), for these pulsars we could instead invert the process and use the h_0 upper limit to set a limit on the spin-down of the pulsars (at least under the assumption that they are gravitars, with $n = 5$). Given that the maximum observed spin-up for a globular cluster pulsar is $\sim 5 \times 10^{-14}$ Hz s^{-1}, we can say that the negative of this can be used as an approximation for the largest magnitude *spin-down* that could be masked by intracluster accelerations.[163] Of the globular cluster pulsars for which the intrinsic spin-down is not known, we find that our upper limits on h_0 give the smallest limit on the absolute spin-down value, due to gravitational waves for PSR J1623 −2631 of $\dot{f} = -3.2 \times 10^{-13}$ Hz s^{-1}. Although this value is probably too large to be masked by accelerations, it is of the same order as the spin-downs for two globular cluster millisecond pulsars, PSRs J1823-3021A (Freire et al. 2011) and J1824-2452A (Johnson et al. 2013), both with apparently large intrinsic spin-down values.

4.1. High-value Targets

Table 2 shows the results for the high-value targets (Section 2.1) for each of the three analysis methods discussed in Section 3. The results from the methods are broadly consistent. For pulsars that have restricted priors on orientations, the results using these are shown alongside the results from the full prior orientation range. We find that for eight of these pulsars, we achieve a sensitivity that surpasses the indirect spin-down limit.

Table 2 also contains an estimate of the maximum surface deformation of the $l = m = 2$ mode, $R\varepsilon_{\text{surf},22}$, for each of the pulsars. This is based on Figure 2 of Johnson-McDaniel (2013), where we adopt a scaling of $R\varepsilon_{\text{surf},22} \approx 25(\varepsilon/10^{-4})$ cm maximized over equations of state and possible stellar masses. We also find that for five of these pulsars (PSRs J0534+2200, J1302−6350, J1813−1246, J1952+3252, and J2229+6114) the $l = m = 2$ surface deformations are smaller than the rotational ($l = 2$, $m = 0$) surface deformation for all equations of state.[164] For the Vela pulsar (PSR J0835−4510) and PSR J0205+6449, the $l = m = 2$ surface deformations are smaller than the rotational deformations for roughly half of the equations of state used in Johnson-McDaniel (2013). There is no expected relation between the scales of these two deformations, but it is intriguing to compare them nonetheless.

5. Discussion

We have searched for gravitational-wave emission from the $l = m = 2$ quadrupole mode of 200 known pulsars. There is no significant evidence for a signal from any of the sources. We

---

[162] This is for PSR J1833−0827 at 23.4 Hz, for which there appears to be a large amount of incoherent interference between the detectors.

[163] In Owen (2006) and Pitkin (2011), it is stated that -5×10^{-13} Hz s^{-1} is roughly the largest magnitude spin-down that could be masked by globular cluster accelerations. This is mainly based on the maximum observed spin-up for a globular cluster pulsar (PSR J2129+1210D) being $\sim 5 \times 10^{-13}$ Hz s^{-1} as given in v1.54 of the ATNF pulsar catalog (Manchester et al. 2005). However, this value appears to be wrong, with the original observations for PSR J2129+1210D (Anderson 1993) giving a value of just under $\sim 5 \times 10^{-14}$ Hz s^{-1}. This is still the maximum observed spin-up for any globular cluster pulsar.

[164] For this we have assumed a 1.4 $M_\odot$ star and used approximate scalings calculated from Table 1 of Johnson-McDaniel (2013), taking into account that the rotational deformation scales with f_{rot}^2.
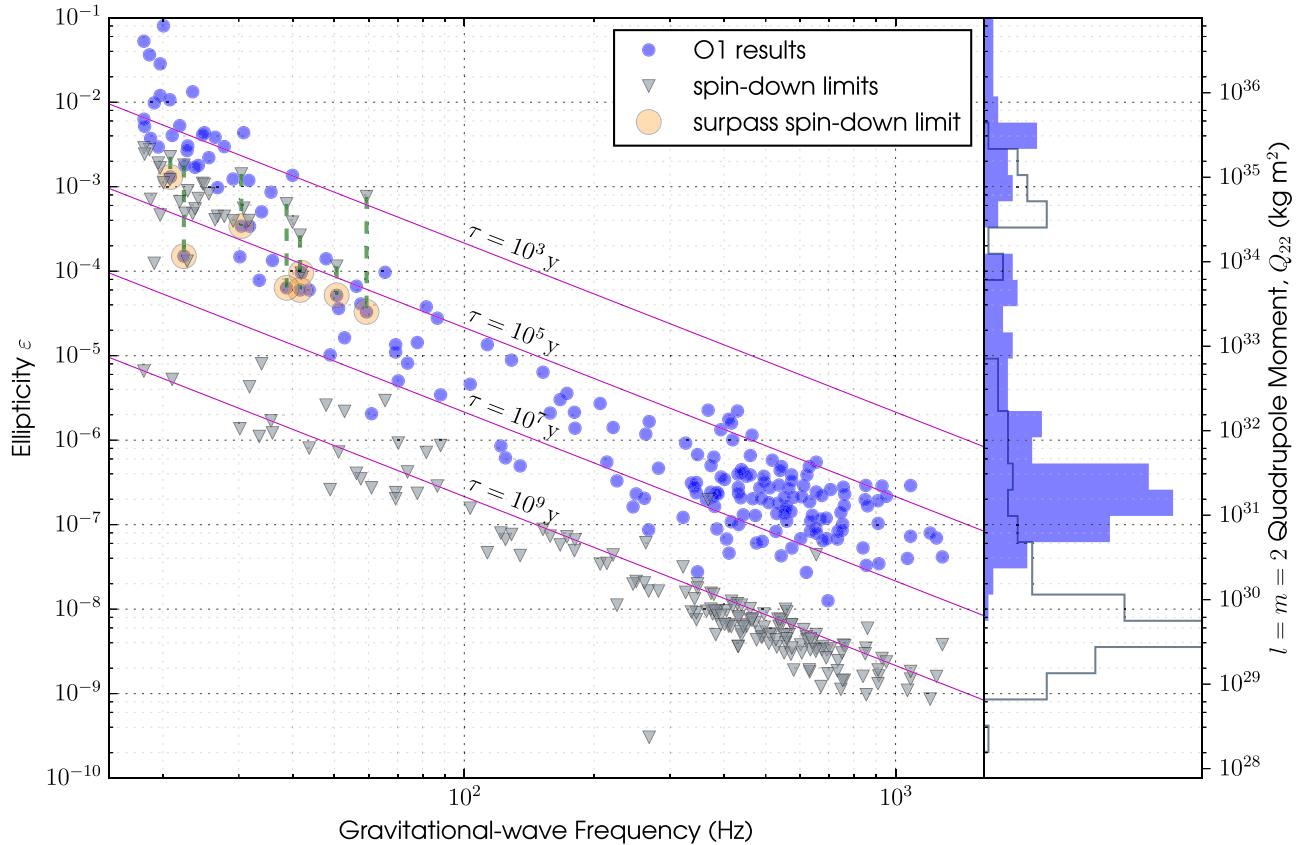
Figure 3. Limits on fiducial ellipticities (ε) and mass quadrupole moments (Q_{22}). ▼ show the values based on the spin-down limits for these pulsars. The pulsars for which the spin-down limit is surpassed are highlighted within larger shaded circles and linked to their spin-down limit values with dashed vertical lines. Also shown are diagonal lines of constant characteristic age, τ, for gravitars (with braking indices of $n = 5$) calculated via $\varepsilon^{\rm sd} = 1.91 \times 10^5 f_{\rm rot}^{-2} / \sqrt{(n - 1)\tau I_{38}}$, where I_{38} is the principal moment of inertia in units of 10^{38} kg m^2 (where we set $I_{38} = 1$).
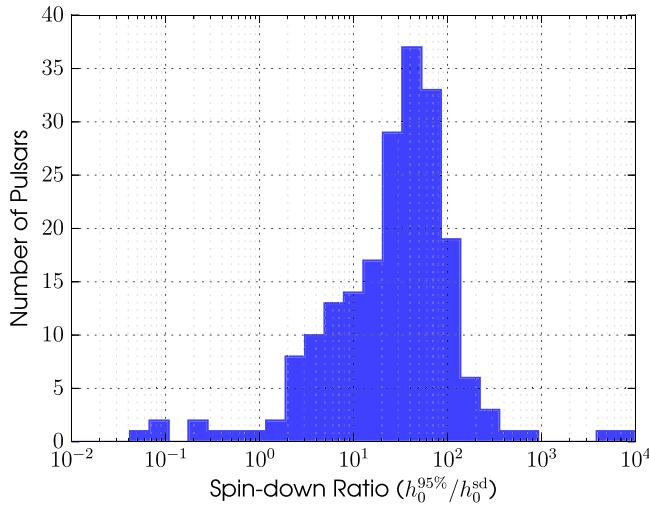
Figure 4. Ratio between our observed $h_0^{95\%}$ limits and the spin-down limits for all pulsars.

have been able to set 95% credible upper limits on the gravitational-wave amplitudes from all these sources, and from these derived limits on each star's fiducial ellipticity and quadrupole moment.

In earlier analyses, the indirect spin-down limits on the gravitational-wave amplitude had been surpassed for two

pulsars: PSR J0534+2200 (the Crab pulsar; Abbott et al. 2008) and PSR J0835−4510 (the Vela pulsar; Abadie et al. 2011). We improve upon the previous limits for these two pulsars by factors of $\gtrsim 3$. We find that for the Crab and Vela pulsars, less than $\sim 2 \times 10^{-3}$ and $\sim 10^{-2}$ of the spin-down luminosity is being lost via gravitational radiation, respectively (assuming the distance is precisely known and using the fiducial moment of inertia of 10^{38} kg m^2). The observed braking indices of these pulsars provide constraints on the contribution of gravitational-wave emission to the spin-down, under the assumption that the spin-down is due only to a combination of electromagnetic and gravitational-wave losses. These braking index constraints are more stringent, i.e., give smaller limits on the gravitational-wave emission, than the naïve spin-down limit given in Equation (1) (see Palomba 2000). Our results, however, surpass even these more stringent limits and are therefore compatible with the observed braking indices. We surpass the spin-down limits of six further pulsars. All these are young pulsars with large spin-down luminosities, and as such our limits translate to large ellipticities/quadrupole moments that are at the upper end of some maximally allowed values (see e.g., Owen 2005; Pitkin 2011; Johnson-McDaniel & Owen 2013). If we assume that internal toroidal magnetic fields are the source of any stellar mass quadrupole (Bonazzola & Gourgoulhon 1996), then we can use our limits on ellipticities as constraints on the magnitude of the internal field strength. For the Crab pulsar,

Table 2
Limits on the Gravitational-wave Amplitude, and Other Derived Quantities, for the 11 High-value Pulsars

Analysis	$h_0^{95\%}$ (10^{-25})	ε (10^{-4})	Q_{22} $(10^{34}\,\mathrm{kg\,m^2})$	$h_0^{95\%}/h_0^{\mathrm{sd}}$	$\dot{E}_{\mathrm{gw}}/\dot{E}$	$R\varepsilon_{\mathrm{surf,22}}$ cm[a]	$\log_{10}\mathcal{O}_{\mathrm{S/I}}$[b]/ FAP[c]/$p$-value[d]
			PSR J0205+6449 (Pre-glitch)				
Bayesian	1.1 (1.3)	3.6 (4.3)	2.8 (3.3)	0.25 (0.31)	0.064 (0.093)	90 (110)	−1.2 (−1.1)
$\mathcal{F}/\mathcal{G}$-statistic	1.8 (2.4)	5.9 (7.9)	4.5 (6.1)	0.42 (0.55)	0.17 (0.31)	150 (200)	0.27 (0.16)
$5n$-vector	0.75 (1.1)	2.5 (3.7)	1.9 (2.8)	0.17 (0.25)	0.030 (0.064)	60 (90)	0.95
			(Post-glitch)				
Bayesian	2.0 (2.6)	6.4 (8.4)	5.0 (6.5)	0.45 (0.60)	0.21 (0.36)	160 (210)	−1.0 (−0.7)
$\mathcal{F}/\mathcal{G}$-statistic	1.7 (1.4)	5.6 (4.6)	4.3 (3.5)	0.39 (0.32)	0.15 (0.10)	140 (120)	0.49 (0.91)
$5n$-vector	1.1 (1.7)	3.6 (5.4)	2.8 (4.2)	0.25 (0.38)	0.065 (0.15)	90 (140)	0.32
			(Incoherently Combined)				
Bayesian	1.0 (1.3)	3.4 (4.4)	2.6 (3.4)	0.24 (0.31)	0.058 (0.097)	90 (110)	−0.6 (−0.5)
$\mathcal{F}/\mathcal{G}$-statistic	1.2 (1.6)	3.9 (5.2)	3.0 (4.0)	0.28 (0.37)	0.077 (0.14)	100 (130)	0.36 (0.48)
$5n$-vector	0.73 (1.1)	2.3 (3.5)	1.8 (2.7)	0.17 (0.25)	0.028 (0.064)	60 (90)	0.95
			PSR J0534+2200 (Crab)				
Bayesian	0.67 (0.61)	0.36 (0.33)	0.28 (0.25)	0.05 (0.04)	0.0022 (0.0018)	9 (8)	−0.7 (−0.7)
$\mathcal{F}/\mathcal{G}$-statistic	0.42 (0.24)	0.23 (0.13)	0.17 (0.10)	0.03 (0.02)	0.00087 (0.00028)	6 (3)	0.62 (0.31)
$5n$-vector	0.52 (0.50)	0.28 (0.27)	0.22 (0.21)	0.04 (0.04)	0.0013 (0.0012)	7 (7)	0.21
			PSR J0835−4510 (Vela)				
Bayesian	3.2 (2.8)	1.7 (1.5)	1.3 (1.2)	0.10 (0.08)	0.0090 (0.0070)	40 (40)	−0.9 (−0.9)
$\mathcal{F}/\mathcal{G}$-statistic	3.8 (3.3)	2.0 (1.7)	1.6 (1.3)	0.11 (0.10)	0.012 (0.0094)	50 (40)	0.37 (0.58)
$5n$-vector	2.9 (2.9)	1.5 (1.5)	1.2 (1.2)	0.09 (0.09)	0.0073 (0.0073)	40 (40)	0.66
			PSR J1302−6350				
Bayesian	0.77	0.96	0.74	1.0	1.0	20	−1.0
$\mathcal{F}$-statistic	0.60	0.74	0.58	0.78	0.61	20	0.44
			PSR J1809−1917				
Bayesian	3.0	18	14	2.5	⋯	450	−1.0
$\mathcal{F}$-statistic	2.4	14	11	2.0	⋯	350	0.72
$5n$-vector	2.5	15	12	2.1	⋯	380	0.62
			PSR J1813−1246				
Bayesian	0.44	0.60	0.46	0.23	0.051	20	−1.2
$\mathcal{F}$-statistic	0.55	0.75	0.58	0.28	0.079	20	0.61
$5n$-vector	0.55	0.75	0.58	0.28	0.079	20	0.69
			PSR J1826−1256				
Bayesian	15	52	40	2.1	⋯	1300	−0.9
$\mathcal{F}$-statistic	17	59	45	2.4	⋯	1500	0.29
$5n$-vector	18	62	48	2.6	⋯	1600	0.21
			PSR J1928+1746				
Bayesian	1.4	12	9.5	3.1	⋯	300	−1.0
$\mathcal{F}$-statistic	1.5	14	11	3.4	⋯	350	0.42
$5n$-vector	1.3	12	9.1	3.0	⋯	300	0.70
			PSR J1952+3252				
Bayesian	0.47 (0.50)	0.52 (0.56)	0.40 (0.43)	0.45 (0.49)	0.20 (0.24)	10 (10)	−1.1 (−1.1)
$\mathcal{F}$-statistic	0.48	0.53	0.41	0.46	0.22	10	0.44
$5n$-vector	0.37 (0.39)	0.41 (0.43)	0.32 (0.33)	0.36 (0.38)	0.13 (0.14)	10 (10)	0.57
			PSR J2043+2740				
Bayesian	5.3	13	10	0.57	0.32	330	−0.8
$\mathcal{F}$-statistic	5.6	14	11	0.61	0.37	350	0.41
$5n$-vector	6.0	15	11	0.65	0.43	380	0.18

Table 2
(Continued)

Analysis	$h_0^{95\%}$ (10^{-25})	ε (10^{-4})	Q_{22} (10^{34} kg m^2)	$h_0^{95\%}/h_0^{sd}$	$\dot{E}_{gw}/\dot{E}$	$R\varepsilon_{surf,22}$ cm[a]	$\log_{10}\mathcal{O}_{S/I}$[b]/ FAP[c]/$p$-value[d]
			PSR J2229+6114				
Bayesian	0.50 (0.34)	0.95 (0.64)	0.73 (0.49)	0.15 (0.10)	0.023 (0.010)	20 (20)	−1.3 (−1.4)
$\mathcal{F}/\mathcal{G}$-statistic	0.49 (0.45)	0.93 (0.85)	0.72 (0.66)	0.15 (0.14)	0.022 (0.018)	20 (20)	0.73 (0.35)
5n-vector	0.56 (0.43)	1.1 (0.84)	0.82 (0.63)	0.17 (0.13)	0.029 (0.017)	30 (20)	0.59

Notes. Limits with constrained orientations (see Appendix B) are given in parentheses. When the spin-down limit is not surpassed, no power ratio, $\dot{E}_{gw}/\dot{E}$, is given.
[a] This is the equivalent upper limit on the $l = m = 2$ surface deformation maximized over the equation of state and stellar mass (Johnson-McDaniel 2013). Values below 10 are rounded to the nearest integer, values between 10 and 1000 are rounded to the nearest decade, and values above 1000 are rounded to the nearest hundred.
[b] For the Bayesian analysis, this column gives the logarithm of the odds for a coherent signal being present in the data versus an incoherent signal or noise being present in the data (Equation (12)).
[c] For the $\mathcal{F}/\mathcal{G}$-statistic analysis, this column gives the false alarm probability. The false alarm probabilities are calculated using the observed values of 2 $\mathcal{F}$ and 2 $\mathcal{G}$, and assuming they are drawn from χ^2 distributions with 4 and 2 degrees of freedom for the $\mathcal{F}$- and $\mathcal{G}$-statistics, respectively.
[d] For the 5n-vector results, this column gives the significance expressed as a p-value representing the probability that noise alone can produce a value of the detection statistic larger than that actually obtained in the analysis (see Aasi et al. 2015 for more discussion of this).

PSR J1813−1246, PSR J1952+3252, and PSR J2229+6114, which have roughly comparable ellipticity limits, the internal magnetic field strength is limited to $\lesssim 10^{16}$ G (e.g., Cutler 2002; Haskell et al. 2008). For comparison, the Crab pulsar's inferred external polar magnetic field at its surface is $\sim 4 \times 10^{12}$ G. Due to this being a rough order of magnitude estimate, this value is the same as that previously quoted for the Crab pulsar in Aasi et al. (2014), although the limit is now valid for several more pulsars.

For any neutron star equation of state, the lower bound on the mass quadrupole (due to the internal magnetic field, which may be very weak) is many orders of magnitude less than the upper bound. Therefore, it is always important to acknowledge that these upper limits on particular stars do not allow us to place constraints on neutron star equations of state.

Of all the pulsars, the smallest 95% credible limit on h_0 that we find is 1.6×10^{-26} for PSR J1918−0642. The smallest ellipticity and Q_{22} quadrupole moments are 1.3×10^{-8} and 9.7×10^{29} kg m^2, respectively, for J0636+5129, which is a relatively nearby pulsar at ~ 0.20 kpc. Although neither of these pulsars surpasses their fiducial spin-down limits, it is interesting to note that there are 32 that we are able to constrain to within a factor of 10 of their spin-down limits (see Figure 4). For PSR J0437−4715 (which is nearby, at 0.16 kpc), we are in fact only 1.4 times above the spin-down limit. Therefore, an equivalent increase in detector sensitivity of that factor, or a $1.4^2 \approx 1.9$ times longer run, would allow us to surpass the spin-down limit. Alternatively, the spin-down limit would be surpassed if the true moment of inertia for PSR J0437−4715 were a factor of 1.9 times larger than I_{38}, which is well within plausible values. As this is a millisecond pulsar, it would give ellipticity constraints of less than a few 10^{-8}, or $l = m = 2$ quadrupole moment constraints of $\lesssim 10^{30}$ kg m^2, compared to the much larger constraints typically found for the young pulsars in Table 1. Using the conversion in Cutler (2002) the constraints on the internal toroidal fields for this pulsar would be $\lesssim 10^{13}$ G, which is similar to the external field strengths of young pulsars.

This search has imposed a model in which the gravitational-wave signal phase evolutions must be tightly locked to the pulsars' rotational evolutions determined through electromagnetic observations. There are mechanisms (discussed in, e.g., Abbott et al. 2008), however, that could lead to small deviations between the phase evolution and observed rotation. Additionally, there are many pulsars for which highly accurate timings do not exist or are not available from observations coincident with ours.[165] There are several such sources for which the spin-down limit could be surpassed and these are being searched for in O1 data using narrow-band searches (see, e.g., Aasi et al. 2015), covering a small range in frequency and frequency derivative to account for uncertainties in the exact parameters (LIGO Scientific Collaboration & Virgo Collaboration 2017, in preparation). All-sky broadband searches for unknown rotating neutron stars are also underway.

In the near future, increasing sensitivities and considerably longer observing runs are planned for aLIGO and Advanced Virgo (Abbott et al. 2016d). This will give us several times greater sensitivity with which to search for gravitational-wave signals, and in any event will allow us to surpass the spin-down limits for 10 or more pulsars. Future searches will also address gravitational-wave emission at not just twice the rotation frequency, but also at the rotation frequency (e.g., Pitkin et al. 2015), further increasing the likelihood of a first detection of continuous gravitational waves.

---

[165] One desirable source that we no longer have accurate timings for is PSR J0537−6910, an X-ray pulsar in the Large Magellanic Cloud, for which we relied on the now-defunct *RXTE* satellite.

Appendix A
The Application of the Bayesian Method

The Bayesian Method used in our known pulsar searches involves a data processing stage and a parameter estimation stage. For a given source, the data processing stage takes calibrated strain data from H1 and L1 (sampled at a rate of 16,384 Hz), heterodynes it to remove a best fit for the source's phase evolution, and then low-pass filters and heavily down-samples the data to one sample per minute (Dupuis & Woan 2005). This leaves a complex time series with a $1/60$ Hz bandwidth, in which a signal would have the form

$$h'(t) = e^{i\Delta\phi(t)} \frac{h_0}{2} \left(\frac{1}{2} F_+(\psi, t)[1 + \cos^2\iota] e^{i\phi_0} \right.$$
$$\left. - i F_\times(\psi, t)\cos\iota\, e^{i\phi_0} \right), \qquad (7)$$

where the remaining modulation will be due to the detector's diurnal antenna pattern and any slowly varying phase difference caused by potential differences between the best-fit phase evolution and the true signal phase evolution $\Delta\phi(t) = (\phi_{\text{true}}(t) - \phi_{\text{best-fit}}(t))$.[166]

---

[166] The analysis code actually works with a signal parameterized in terms of the "waveform" model defined in Jones (2015) and Pitkin et al. (2015), where $h_0 = -2C_{22}$ and $\phi_0 = \Phi_{22}^C$.

These combined processed data sets for each detector $\boldsymbol{d}$ are used to estimate the joint posterior probability distribution of the unknown source signal parameters, $\boldsymbol{\theta}$, using a Bayesian framework via

$$p(\boldsymbol{\theta}|\boldsymbol{d}, H_{\text{S}}, I) = \frac{p(\boldsymbol{d}|\boldsymbol{\theta}, H_{\text{S}}, I)p(\boldsymbol{\theta}|H_{\text{S}}, I)}{p(\boldsymbol{d}|H_{\text{S}}, I)}, \qquad (8)$$

where $p(\boldsymbol{d}|\boldsymbol{\theta}, H_{\text{S}}, I)$ is the likelihood of the data given the specific signal model (H_{S}) parameters, $p(\boldsymbol{\theta}|H_{\text{S}}, I)$ is the joint prior probability distribution of the parameters, and $p(\boldsymbol{d}|H_{\text{S}}, I)$ is the evidence (marginal likelihood) of observing our data, given a signal of the type we defined. In the cases where $\Delta\phi(t)$ are negligible, this corresponds to just estimating four parameters, $\boldsymbol{\theta} = \{h_0, \phi_0, \cos\iota, \psi\}$. In general, offsets between the best-fit phase parameters and true signal parameters can also be estimated, provided that they do not cause the signal to drift out of the bandwidth available. When using timing solutions calculated using TEMPO(2), uncertainties in the fitted parameters are produced, and when available these fitted parameters will be included in our estimation for the gravitational-wave signal.

In previous searches (e.g., Abbott et al. 2010; Aasi et al. 2014), a Markov Chain Monte Carlo (MCMC) method has been used to sample and estimate $p(\boldsymbol{\theta}|\boldsymbol{d}, H_{\text{S}}, I)$ for the unknown parameters. However, the simple proposal distribution used for the MCMC was not well-tuned and was therefore inefficient, especially when searching over additional phase parameters. Furthermore, the MCMC did not naturally produce a value for the evidence $p(\boldsymbol{d}|H_{\text{S}}, I)$. To allow the calculation of $p(\boldsymbol{d}|H_{\text{S}}, I)$ and, as a natural by-product, the joint parameter posterior probability distribution, we have adopted the nested sampling method (Skilling 2006). In particular our analysis code (Pitkin et al. 2012; M. Pitkin et al. 2017, in preparation) uses the nested sampling implementation of Veitch & Vecchio (2010) as provided in the LALInference library (Veitch et al. 2015) within the LIGO Algorithm Library (LAL) suite.[167] This implements more intelligent and efficient proposals than previously used. The code has been validated by extracting both software and hardware (Biwer et al. 2016) signal injections into gravitational-wave detector data.

A.1. The Likelihood

The likelihood, $p(\boldsymbol{d}|\boldsymbol{\theta}, H_{\text{S}}, I)$, is a Student's t-like probability distribution and is given in, e.g., Abbott et al. (2007). It assumes that the noise in the data may be non-stationary, but consists of stationary Gaussian segments, each with unknown variance. The analysis uses a Bayesian Blocks-type method (Scargle 1998) to divide the data into stationary segments, although those containing fewer than five points are discarded. Any segments longer than a day (1440 points given our $1/60$ Hz sample rate) are split such that no segments are longer than 1440 points. This differs from previous analyses in which the data were automatically split into segments containing 30 points.

In cases where the search requires the recalculation of $\Delta\phi(t)$ when evaluating the likelihood, this can be computationally

---

[167] https://wiki.ligo.org/DASWG/LALSuite

expensive; the phase, including solar system and binary system barycentring time delays, is needed and the log-likelihood calculation requires summations over all data points. To make this considerably more efficient, we have adopted a Reduced Order Quadrature scheme (e.g., Antil et al. 2013; Canizares et al. 2013) to approximate the likelihood via interpolation of a reduced model basis.

A.2. The Priors

In Equation (8), a prior probability distribution for the parameters is required. For the parameters ϕ_0, $\cos\iota$, and ψ, we generally have no prior knowledge of their values, and so use flat priors within their allowed ranges:

$$
p(\phi_0|H_S, I) = \begin{cases} 1/2\pi & \text{if } 0 \leqslant \phi_0 \leqslant 2\pi, \\ 0 & \text{otherwise,} \end{cases}
$$

$$
p(\cos\iota|H_S, I) = \begin{cases} 1/2 & \text{if } -1 \leqslant \cos\iota \leqslant 1, \\ 0 & \text{otherwise,} \end{cases}
$$

$$
p(\psi|H_S, I) = \begin{cases} 2/\pi & \text{if } 0 \leqslant \psi \leqslant \pi/2, \\ 0 & \text{otherwise.} \end{cases} \tag{9}
$$

These ranges do not necessarily span the full physically allowable range of source values, but are a degenerate range that will contain all possible observable signal waveforms (Jones 2015; Pitkin et al. 2015). In some cases, there is information about the inclination and/or polarization angle of the source (see Appendix B). Where present this can be incorporated into the prior by using a Gaussian distribution based on this information. For the cases where the inclination is recovered from a PWN image, there is no information about the rotation direction of the source, so in fact a bimodal Gaussian prior on ι is required (Jones 2015; see Appendix B).[168]

For a prior on the gravitational-wave amplitude h_0, the analysis in Aasi et al. (2014) used a flat distribution bounded at zero and some value that was large compared to the observed standard deviation of the data, or a distribution on h_0 and $\cos\iota$ based on previous searches (e.g., Abbott et al. 2010). In this analysis, inspired by that used in Middleton et al. (2016), we have adopted a different prior based on the Fermi–Dirac distribution:

$$
p(h_0|\sigma, \mu, H_S, I) = \frac{1}{\sigma \log(1 + e^{\mu/\sigma})}(e^{(h_0-\mu)/\sigma} + 1)^{-1}, \tag{10}
$$

where μ gives the point at which the distribution falls to half its maximum value, and σ defines the rate at which the distribution falls off. If we define a value $u^{95\%}$ at which the cumulative distribution function of Equation (10) is at 95%, and require that the probability density function falls from 97.5% to 2.5% of its maximum over a range that is 0.4 μ, we are able to define μ and σ. In this analysis, there are two ways in which we define $u^{95\%}$ to calculate μ and σ: for pulsars where we already have a 95% h_0 upper limit from previous searches, we use this value as $u^{95\%}$; for new pulsars, we have based $u^{95\%}$ on the the 95% upper limit that would have been

expected if the pulsar had been searched for in the previous S6/VSR2,4 analysis.[169] For small values of h_0 this prior looks flat, while for large values it approximates an exponential distribution. Unlike the flat priors used previously, it is continuous for positive values and penalizes excessively large values.

If searching over the phase parameters defining $\Delta\phi(t)$ in Equation (7), i.e., frequency, sky position, and binary system parameters, the prior distribution on the parameters is based on the uncertainties provided by the TEMPO(2) fits to TOAs. We take the uncertainties as the standard deviations for a multivariate Gaussian prior on these parameters. We conservatively have the parameters as uncorrelated, except in two specific cases for low eccentricity ($e < 10^{-3}$) binary systems. If there are uncertainties on the time and angle of periastron, or if there are uncertainties on the binary period and time derivative of the angle of periastron, then these pairs of parameters are set to be fully correlated.

A.3. The Evidence

The evidence allows a Bayesian model comparison to be performed, i.e., the comparison of the relative probabilities of different signal models given the data, which provides a way of assessing if an observed signal is real (see, e.g., the $\mathcal{B}$-statistic of Prix & Krishnan 2009, for the use of a Bayesian model comparison in this context). For example, we can calculate the ratio of the probability that the data contains a signal to the probability that the data is purely Gaussian noise:

$$
\mathcal{O}_{S/N} = \frac{p(H_S|\boldsymbol{d}, I)}{p(H_N|\boldsymbol{d}, I)} = \frac{p(\boldsymbol{d}|H_S, I)}{p(\boldsymbol{d}|H_N, I)} \frac{p(H_S|I)}{p(H_N|I)}, \tag{11}
$$

where the first term on the right-hand side is called the Bayes factor and $p(H_S|I)/p(H_N|I)$ is the prior odds of the two models, which we set to unity. To calculate $p(\boldsymbol{d}|H_N, I)$ the likelihood can be evaluated with the signal set to zero.

Given more than one detector, we are also able to compare the probability that the data contain a coherent signal between detectors (as would be expected from an astrophysical source) versus independent (and therefore incoherent) signals in each detector *or* the data consisting of non-stationary (see Appendix A.1) Gaussian noise alone (e.g., Keitel et al. 2014). If we take the combined data to be $\boldsymbol{d} = \{\boldsymbol{d}_{H1}, \boldsymbol{d}_{L1}\}$, then we can form four incoherent-signal-or-noise hypotheses (where for compactness we have removed the implicit I dependence):

[H_{N_1}] an independent signal in both detectors, $p(\boldsymbol{d}|H_{N_1}) = p(\boldsymbol{d}_{H1}|H_{S_{H1}})p(\boldsymbol{d}_{L1}|H_{S_{L1}})$;

[H_{N_2}] a signal in H1, but non-stationary Gaussian noise in L1, $p(\boldsymbol{d}|H_{N_2}) = p(\boldsymbol{d}_{H1}|H_{S_{H1}})p(\boldsymbol{d}_{L1}|H_{N_{L1}})$;

[H_{N_3}] a signal in L1, but non-stationary Gaussian noise in H1, $p(\boldsymbol{d}|H_{N_3}) = p(\boldsymbol{d}_{H1}|H_{N_{H1}})p(\boldsymbol{d}_{L1}|H_{S_{L1}})$;

[H_{N_4}] independent non-stationary Gaussian noise in both detectors, $p(\boldsymbol{d}|H_{N_4}) = p(\boldsymbol{d}_{H1}|H_{N_{H1}})p(\boldsymbol{d}_{L1}|H_{N_{L1}})$,

---

[168] A bimodal prior was *not* used in Aasi et al. (2014), but subsequently its inclusion was found to have minimal effect on the upper limits produced.

[169] For two pulsars, PSR J0024−7204X and PSR J0721−2038, the priors set using an estimated 95% upper limit from the S6/VSR2,4 analysis were found to be too narrow and unduly narrowed the posterior. So, to maintain a more conservative upper limit dominated by the likelihood, as has been the case in previous searches, the priors were widened by a factor of three.

Table 3
Means and Standard Deviations for Restricted Priors on ψ and ι Based on Table 2 of Ng & Romani (2008)

PSR	ψ (rad)	ι_1 (rad)	ι_2 (rad)
J0205+6449	1.5760 ± 0.0078	1.5896 ± 0.0219	1.5519 ± 0.0219
J0534+2200 (Crab)	2.1844 ± 0.0016	1.0850 ± 0.0149	2.0566 ± 0.0149
J0835−4510 (Vela)	2.2799 ± 0.0015	1.1048 ± 0.0105	2.0368 ± 0.0105
J1709−4429 (B1706−44)	2.8554 ± 0.0305	0.9303 ± 0.0578	2.2113 ± 0.0578
J1952+3252	−0.2007 ± 0.1501	…	…
J2229+6114	1.7977 ± 0.0454	0.8029 ± 0.1100	2.3387 ± 0.1100

Note. For PSR J1952+3252, the values for ψ are not from PWN fitting but are from the mean of a value derived from proper motion measurements and observations of Hα "lobes" bracketing the bow shock (Ng & Romani 2004).

Table 4
Limits on the Gravitational-wave Amplitude, and Other Derived Quantities, for Known Pulsars

PSR	f (Hz)	d (kpc)	$h_0^{\rm sd}$ (10^{-25})	$h_0^{95\%}$ (10^{-25})	ε (10^{-7})	Q_{22} $(10^{31}$ kg m$^2)$	Spin-down Ratio	$\log_{10}(\mathcal{O}_{\rm S/N})$	$\log_{10}(\mathcal{O}_{\rm S/I})$
J0023+0923	655.69	1.0	0.016	0.36	0.79	0.61	23	−0.5	−1.0
J0024−7204AA	1083.79	4.0	0.0057[b]	0.90	2.9	2.2	160	0.0	−0.5
J0024−7204AB	539.86	4.0	0.0057[b]	0.33	4.4	3.4	58	−0.4	−0.9
J0024−7204C	347.42	4.0	0.0057[b]	0.22	6.8	5.2	38	−1.1	−1.2
J0024−7204D	373.30	4.0	0.0057[b]	0.18	5.0	3.9	32	−0.5	−0.8
J0024−7204E	565.56	4.0	0.0042[a]	0.23	2.7	2.1	54	−0.9	−1.0
J0024−7204F	762.32	4.0	0.0057[b]	0.35	2.3	1.8	62	−0.5	−0.8
J0024−7204G	495.00	4.0	0.0057[b]	0.24	3.7	2.9	43	−0.7	−0.9
J0024−7204H	622.99	4.0	0.0044[a]	0.40	3.9	3.0	90	−0.1	−0.6
J0024−7204I	573.89	4.0	0.0057[b]	0.34	3.9	3.0	60	−0.4	−0.7
J0024−7204J	952.09	4.0	0.0057[b]	0.52	2.2	1.7	91	−0.3	−0.7
J0024−7204L	460.18	4.0	0.0057[b]	0.22	3.9	3.0	38	−0.5	−0.8
J0024−7204M	543.97	4.0	0.0057[b]	0.38	4.9	3.8	67	−0.3	−0.7
J0024−7204N	654.89	4.0	0.0057[b]	0.28	2.4	1.9	49	−0.5	−0.8
J0024−7204O	756.62	4.0	0.0057[b]	0.42	2.8	2.1	74	−0.3	−0.8
J0024−7204Q	495.89	4.0	0.0040[a]	0.21	3.2	2.5	53	−0.5	−1.0
J0024−7204R	574.64	4.0	0.0057[b]	0.29	3.3	2.5	51	−0.3	−0.8
J0024−7204S	706.61	4.0	0.0045[a]	0.34	2.6	2.0	77	−0.4	−0.8
J0024−7204T	263.56	4.0	0.011[a]	0.22	12	9.1	19	−0.4	−0.8
J0024−7204U	460.53	4.0	0.0042[a]	0.37	6.6	5.1	88	0.1	−0.4
J0024−7204W	850.22	4.0	0.0057[b]	0.38	2.0	1.5	66	−0.6	−1.2
J0024−7204X	419.15	4.0	0.0051[a]	0.47	10	7.8	93	−0.2	−0.5
J0024−7204Y	910.47	4.0	0.0029[a]	0.42	1.9	1.5	150	−0.4	−0.7
J0024−7204Z	439.13	4.0	0.0057[b]	0.23	4.5	3.5	40	−0.5	−0.8
J0030+0451	411.06	0.3	0.039	0.27	0.46	0.36	7.1	−0.6	−0.8
J0034−0534	1065.43	1.0	0.013	0.49	0.40	0.31	36	−0.8	−1.0
J0102+4839	674.74	4.0	0.0039	0.26	2.2	1.7	67	−0.7	−0.9
J0218+4232	860.92	3.1	0.015	0.42	1.7	1.3	28	−0.5	−0.8
J0340+4130	606.18	2.7	0.0044	0.31	2.1	1.7	70	−0.5	−0.9
J0348+0432	51.12	2.1	0.0095	0.48	360	280	50	−0.8	−0.9
J0407+1607	77.82	4.1	0.0037	0.22	140	110	61	−0.6	−1.0
J0437−4715	347.38	0.2	0.16	0.22	0.28	0.21	1.4	−1.0	−1.1
J0453+1559	43.69	1.8	0.0089	0.66	600	460	74	−0.8	−1.0
J0605+37	733.15	1.2	0.0091	0.33	0.67	0.52	36	−0.6	−0.8
J0609+2130	35.91	1.8	0.0091	1.0	1300	1000	110	−0.9	−1.2
J0610−2100	517.96	5.6	0.0026	0.29	5.8	4.5	110	−0.7	−0.9
J0613−0200	653.20	1.1	0.013	0.37	0.90	0.70	28	−0.3	−0.7
J0614−3329	635.19	1.0	0.019	0.46	1.1	0.85	25	−0.2	−0.7
J0621+1002	69.31	1.9	0.0055	0.30	110	85	54	−0.8	−1.0
J0636+5129	697.12	0.2	0.044	0.32	0.13	0.097	7.3	−0.6	−0.8
J0645+5158	225.90	0.8	0.0078	0.23	3.3	2.5	30	−0.2	−0.7
J0711−6830	364.23	1.0	0.013	0.27	2.0	1.5	21	−0.3	−0.7
J0721−2038	128.68	3.9	0.0035	0.40	89	68	120	−0.2	−0.7
J0737−3039A	88.11	1.1	0.065	0.26	34	27	4.0	−0.6	−0.9
J0742+66	693.06	0.9	0.019	0.40	0.68	0.53	21	−0.6	−0.8
J0751+1807	574.92	0.4	0.030	0.46	0.53	0.41	15	0.3	−0.6
J0900−3144	180.02	0.8	0.021	0.89	21	17	43	−0.6	−1.0
J0908−4913	18.73	1.0	2.6	14	37,000	29,000	5.3	−0.7	−0.9

Table 4
(Continued)

PSR	f (Hz)	d(kpc)	$h_0^{\rm sd}$ (10^{-25})	$h_0^{95\%}$ (10^{-25})	ε (10^{-7})	Q_{22} $(10^{31}\ {\rm kg\ m^2})$	Spin-down Ratio	$\log_{10}(\mathcal{O}_{\rm S/N})$	$\log_{10}(\mathcal{O}_{\rm S/I})$
J0931−1902	431.22	3.6	0.0020	0.21	4.0	3.1	110	−0.6	−0.9
J0940−5428	22.84	4.3	1.2	3.9	30,000	23,000	3.4	−0.7	−1.0
J1012+5307	380.54	0.7	0.021	0.36	1.6	1.3	17	−0.0	−0.8
J1016−5819	22.77	4.6	0.16	3.2	27,000	21,000	20	−0.7	−1.2
J1016−5857	18.62	9.3	1.1	14	360,000	280,000	13	−0.9	−1.1
J1017−7156	855.24	0.7	0.011	0.36	0.33	0.25	34	−0.7	−0.9
J1022+1001	121.56	0.7	0.017	0.18	8.5	6.6	11	−0.7	−1.0
J1024−0719	387.43	1.1	0.014	0.33	2.3	1.8	24	−0.1	−0.5
J1028−5819	21.88	2.8	1.2	9.7	53,000	41,000	7.9	0.6	−0.6
J1038+0032	69.32	2.4	0.0052	0.29	130	100	56	−0.9	−1.0
J1045−4509	267.59	0.3	0.036	0.19	0.87	0.67	5.3	−0.4	−0.8
J1055−6028	20.07	30.0	0.16	11	800,000	620,000	72	−1.1	−1.3
J1105−6107	31.65	7.1	0.60	1.8	12,000	9200	3.0	−0.8	−1.0
J1112−6103	30.78	30.0	0.19	1.5	44,000	34,000	7.8	−1.7	−1.7
J1122+78	476.01	0.6	0.016	0.23	0.61	0.47	14	−0.6	−0.9
J1125−6014	760.35	1.9	0.0045	0.53	1.7	1.3	120	−0.2	−0.6
J1142+0119	394.07	2.0	0.0068	0.29	3.7	2.8	43	−0.3	−0.6
J1231−1411	542.91	0.5	0.044	0.30	0.43	0.33	6.7	−0.6	−0.8
J1300+1240	321.62	0.6	0.058	0.22	1.2	0.94	3.9	−0.6	−0.9
J1302−3258	530.38	1.9	0.0057	0.22	1.4	1.0	38	−0.7	−1.0
J1312+0051	473.03	1.1	0.014	0.26	1.3	0.99	18	−0.5	−1.1
J1327−0755	746.85	2.2	0.0031	0.38	1.4	1.1	120	−0.5	−0.8
J1410−6132	39.96	30.0	0.21	0.77	14,000	11,000	3.6	−1.0	−1.1
J1418−6058	18.08	1.6	6.2	14	63,000	49,000	2.2	0.2	−0.5
J1446−4701	911.29	2.0	0.0082	0.45	1.0	0.80	54	−0.4	−1.1
J1453+1902	345.29	0.9	0.012	0.32	2.4	1.8	26	−0.7	−0.8
J1455−3330	250.40	0.7	0.019	0.21	2.3	1.8	11	−0.5	−0.8
J1509−5850	22.49	3.9	0.67	2.5	18,000	14,000	3.7	−1.0	−1.1
J1518+4904	48.86	0.7	0.0094	0.37	100	79	39	−1.1	−1.2
J1524−5625	25.57	3.8	1.5	4.0	22,000	17,000	2.7	−0.5	−0.8
J1531−5610	23.75	3.1	1.1	3.3	17,000	13,000	3.1	−0.6	−1.1
J1537+1155	52.76	1.1	0.061	0.46	160	130	7.4	−0.3	−0.7
J1545−4550	559.40	2.0	0.015	0.27	1.6	1.3	18	−0.6	−0.9
J1551−0658	281.94	1.5	0.0094	0.27	4.7	3.6	28	−0.3	−1.0
J1600−3053	555.88	1.8	0.0073	0.27	1.5	1.2	38	−0.6	−1.0
J1603−7202	134.75	0.5	0.016	0.18	5.0	3.8	11	−0.3	−0.9
J1614−2230	634.76	0.7	0.020	0.51	0.84	0.65	25	0.4	−0.1
J1618−3921	166.84	4.8	0.0036	0.19	30	23	52	−0.4	−0.8
J1623−2631	180.57	1.8	0.013[b]	0.27	14	11	21	−0.3	−0.7
J1630+37	602.75	0.8	0.017	0.31	0.68	0.53	18	−0.5	−0.8
J1640+2224	632.25	1.4	0.0053	0.54	1.9	1.4	100	0.3	−0.3
J1643−1224	432.75	0.7	0.022	0.27	1.0	0.77	12	−0.3	−0.7
J1653−2054	484.36	2.6	0.0050	0.26	2.7	2.1	51	−0.5	−0.9
J1708−3506	443.94	3.5	0.0037	0.25	4.2	3.2	68	−0.5	−0.9
J1709+2313	431.85	1.8	0.0039	0.30	2.8	2.1	76	−0.6	−0.9
J1709−4429	19.51	2.6	3.0	6.1	40,000	31,000	2.1	−0.7	−1.0
J1709−4429[c]	19.51	2.6	3.0	4.6	30,000	23,000	1.5	−0.8	−1.0
J1710+49	621.07	0.4	0.049	0.28	0.27	0.21	5.8	−0.6	−1.0
J1713+0747	437.62	1.2	0.0093	0.36	2.1	1.6	38	0.1	−0.4
J1718−3825	26.78	4.2	0.80	1.7	9800	7500	2.2	−0.8	−1.1
J1719−1438	345.41	1.6	0.0058	0.24	3.1	2.4	42	−1.0	−1.1
J1721−2457	571.98	1.6	0.0065	0.32	1.4	1.1	49	−0.5	−0.8
J1727−2946	73.85	1.6	0.015	0.29	82	63	19	−0.8	−1.1
J1729−2117	30.17	1.4	0.0093	1.0	1500	1100	110	−1.0	−1.1
J1730−2304	246.22	0.6	0.020	0.17	1.6	1.3	8.2	−0.7	−1.1
J1731−1847	853.04	4.0	0.0066	0.56	2.9	2.3	84	−0.5	−0.7
J1732−5049	376.47	1.8	0.0073	0.18	2.1	1.6	24	−0.7	−0.9
J1738+0333	341.87	1.5	0.011	0.23	2.8	2.1	21	−0.9	−1.1
J1741+1351	533.74	1.1	0.021	0.50	1.8	1.4	24	0.5	−0.2
J1744−1134	490.85	0.4	0.030	0.40	0.63	0.49	13	−0.0	−0.5
J1745+1017	754.11	1.4	0.0063	0.45	1.0	0.79	71	0.1	−0.4
J1745−0952	103.22	2.4	0.0074	0.22	46	35	29	−0.7	−0.9
J1748−2446A	172.96	5.5	0.0041[b]	0.21	36	28	50	−0.4	−0.9

Table 4
(Continued)

PSR	f (Hz)	d (kpc)	$h_0^{\rm sd}$ (10^{-25})	$h_0^{95\%}$ (10^{-25})	ε (10^{-7})	Q_{22} $(10^{31}~{\rm kg~m^2})$	Spin-down Ratio	$\log_{10}(\mathcal{O}_{\rm S/N})$	$\log_{10}(\mathcal{O}_{\rm S/I})$
J1748−3009	206.53	6.0	0.0026	0.21	27	21	79	−0.4	−0.8
J1750−2536	57.55	3.5	0.0035	0.41	410	320	120	−0.8	−1.0
J1751−2857	510.87	1.4	0.0095	0.52	2.7	2.1	55	−0.1	−0.6
J1753−1914	31.77	2.8	0.016	1.3	3400	2600	80	−0.5	−0.7
J1753−2240	21.02	3.5	0.0071	5.5	40,000	31,000	770	−0.8	−1.0
J1756−2251	70.27	0.7	0.066	0.36	50	39	5.4	−0.5	−1.0
J1757−27	113.08	5.4	0.0012	0.34	140	100	290	−0.2	−0.5
J1801−1417	551.71	1.8	0.0054	0.38	2.1	1.6	69	−0.4	−0.7
J1801−3210	268.33	5.1	0.000046	0.25	17	13	5500	−0.3	−0.8
J1802−2124	158.13	3.3	0.0058	0.17	21	16	29	−0.7	−0.9
J1804−0735	86.58	7.8	0.0029[b]	0.28	280	210	97	−0.7	−0.9
J1804−2717	214.06	1.2	0.014	0.23	5.5	4.3	16	0.2	−0.5
J1810+1744	1202.82	2.5	0.0053	0.49	0.80	0.61	92	−0.6	−0.9
J1811−2405	751.71	1.7	0.011	0.30	0.86	0.66	28	−0.7	−0.9
J1813−2621	451.47	3.4	0.0040	0.24	3.7	2.9	60	−0.5	−0.8
J1823−3021A	367.65	8.6	0.023	0.27	23	17	11	−0.3	−0.9
J1824−2452A	654.81	5.1	0.036	0.45	5.5	4.2	12	−0.0	−0.5
J1825−0319	439.22	3.3	0.0031	0.26	4.1	3.2	83	−0.5	−0.8
J1826−1334	19.71	4.1	1.7	12	120,000	93,000	7.2	−0.3	−0.7
J1828−1101	27.76	7.3	0.50	3.3	30,000	23,000	6.7	−0.6	−0.9
J1832−0836	735.53	1.4	0.010	0.34	0.83	0.64	34	−0.6	−0.9
J1833−0827	23.45	4.5	0.62	17	130,000	100,000	28	12.4	−5.5
J1837−0604	20.77	6.2	0.89	7.9	110,000	83,000	8.8	−0.4	−0.7
J1840−0643	56.21	6.7	0.0020	0.33	660	510	160	−1.0	−1.1
J1843−1113	1083.62	2.0	0.0094	0.46	0.73	0.56	49	−0.7	−1.0
J1845−0743	19.10	5.8	0.082	6.5	98,000	76,000	79	−0.8	−1.0
J1853+1303	488.78	1.6	0.0074	0.32	2.0	1.6	43	−0.6	−0.9
J1853−0004	19.72	6.6	0.29	18	280,000	220,000	62	−0.2	−0.6
J1856+0245	24.72	10.3	0.69	2.6	41,000	32,000	3.7	−0.8	−1.0
J1857+0943	372.99	0.7	0.021	0.51	2.4	1.9	24	0.3	−0.6
J1903+0327	930.27	6.5	0.0037	0.41	2.9	2.2	110	−0.8	−1.0
J1903−7051	555.88	1.1	0.029	0.42	1.4	1.1	14	−0.3	−0.8
J1909−3744	678.63	1.1	0.015	0.28	0.65	0.50	18	−0.6	−0.9
J1910+1256	401.32	1.9	0.0058	0.30	3.4	2.7	52	−0.6	−0.9
J1910−5959A	612.33	4.5	0.0051[b]	0.26	2.9	2.2	50	0.0	−0.5
J1910−5959C	378.98	4.5	0.0051[b]	0.21	6.3	4.9	42	−0.4	−1.2
J1910−5959D	221.35	4.5	0.0051[b]	0.16	14	11	32	−0.3	−0.8
J1911+1347	432.34	1.6	0.0096	0.29	2.4	1.8	30	−0.4	−0.7
J1911−1114	551.61	1.6	0.010	0.27	1.3	1.0	27	−0.6	−1.2
J1915+1606	33.88	7.1	0.014	0.86	5000	3900	63	−0.8	−1.0
J1918−0642	261.58	0.9	0.016	0.16	2.1	1.6	10	−0.7	−0.9
J1923+2515	527.96	1.0	0.013	0.25	0.83	0.64	19	−0.7	−1.1
J1925+1721	26.43	9.6	0.31	3.0	38,000	30,000	9.5	−0.6	−0.7
J1932+17	47.81	2.7	0.023	1.3	1400	1100	54	1.6	0.9
J1935+2025	24.96	8.6	0.81	3.3	44,000	34,000	4.1	−0.6	−1.0
J1939+2134	1283.86	1.5	0.044	0.48	0.42	0.32	11	−0.7	−1.0
J1943+2210	393.38	8.3	0.0013	0.26	13	10	200	−0.4	−0.8
J1944+0907	385.71	1.3	0.012	0.30	2.4	1.9	26	−0.4	−0.7
J1946+3417	630.89	6.4	0.0013	0.32	4.9	3.8	260	−0.5	−0.8
J1949+3106	152.23	7.8	0.0028	0.20	64	49	72	−0.5	−0.8
J1950+2414	464.60	7.3	0.0023	0.36	11	8.9	150	−0.2	−0.7
J1955+2527	410.44	9.1	0.0012	0.35	18	14	280	−0.0	−0.6
J1955+2908	326.10	5.4	0.0033	0.19	9.2	7.1	58	−0.7	−0.9
J1959+2048	1244.24	1.5	0.017	0.74	0.69	0.54	44	−0.4	−0.8
J2007+2722	81.64	6.8	0.0074	0.39	380	290	53	−0.4	−0.9
J2010−1323	382.90	1.3	0.0060	0.28	2.3	1.8	46	−0.5	−0.8
J2017+0603	690.56	1.3	0.010	0.46	1.2	0.92	45	−0.4	−1.1
J2019+2425	508.32	0.9	0.012	0.55	1.8	1.4	46	−0.1	−0.7
J2033+1734	336.19	1.4	0.0081	0.27	3.1	2.4	34	−0.6	−1.0
J2043+1711	840.38	1.2	0.0096	0.32	0.53	0.41	33	−0.6	−1.0
J2047+1053	466.64	2.2	0.0080	0.21	2.0	1.6	26	−0.7	−0.9
J2051−0827	443.59	1.3	0.011	0.21	1.3	1.0	20	−0.7	−0.9
J2124−3358	405.59	0.4	0.041	0.29	0.68	0.52	7.1	−0.3	−1.0

Table 4
(Continued)

PSR	f (Hz)	d (kpc)	h_0^{sd} (10^{-25})	$h_0^{95\%}$ (10^{-25})	ε (10^{-7})	Q_{22} $(10^{31}\,\mathrm{kg\,m^2})$	Spin-down Ratio	$\log_{10}(\mathcal{O}_{S/N})$	$\log_{10}(\mathcal{O}_{S/I})$
J2129+1210A	18.07	12.9	0.0018[b]	14	530,000	410,000	8000	−0.6	−0.8
J2129+1210B	35.63	12.9	0.0018[b]	0.90	8600	6700	510	−1.1	−1.2
J2129+1210C	65.51	10.0	0.010[a]	0.34	970	750	33	−0.8	−1.0
J2129+1210D	416.42	12.9	0.0018[b]	0.23	16	12	130	−0.6	−0.9
J2129+1210E	429.97	12.9	0.0018[b]	0.34	22	17	190	−0.1	−0.5
J2129−5721	536.72	3.2	0.0060	0.28	2.9	2.3	47	0.1	−0.4
J2145−0750	124.59	0.5	0.021	0.19	6.2	4.8	9.2	−0.4	−0.8
J2214+3000	641.18	1.0	0.018	0.56	1.3	1.0	32	−0.1	−0.6
J2222−0137	60.94	0.3	0.040	0.30	21	16	7.5	−1.1	−1.2
J2229+2643	671.63	1.4	0.0040	0.39	1.2	0.90	96	−0.4	−0.9
J2234+06	559.19	1.1	0.013	0.32	1.1	0.85	25	−0.5	−0.8
J2235+1506	33.46	1.1	0.011	0.80	780	600	71	−1.0	−1.1
J2241−5236	914.62	0.7	0.021	0.45	0.35	0.27	21	−0.5	−0.9
J2302+4442	385.18	0.8	0.018	0.19	0.89	0.69	11	−0.1	−0.4
J2317+1439	580.51	1.9	0.0036	0.40	2.1	1.6	110	−0.2	−0.6
J2322+2057	415.94	0.8	0.015	0.25	1.1	0.84	17	−0.6	−0.8

Notes. This does not include the high-value targets already listed in Table 2. For PSR J0023+0923 and PSR J0340+4130, intrinsic period derivatives are available in the ATNF pulsar catalog (v. 1.54) (Manchester et al. 2005); however, they are incorrect and therefore the spin-down limits have been calculated using the observed spin-down. For eight pulsars in the globular cluster 47 Tuc (PSRs J0024−7204E, H, Q, S, T, U, X, and Y). we have obtained (P. C. C. Freire 2016, private communication) intrinsic period derivatives to calculate the spin-down limits, with that for X being the 3σ upper limit from Ridolfi et al. (2016) given that it gives a characteristic age older than 10^9 years. For PSR J1823−3021A (in globular cluster NGC 6624) and PSR J1824−2452A (in globular cluster M28), we follow Freire et al. (2011) and Johnson et al. (2013) and calculate the spin-down limit assuming that the contributions to the observed $\dot{f}_{rot}$ are negligibly affected by cluster accelerations. The intrinsic spin-down for PSR J2129+1210C (in globular cluster M15) is taken from McNamara et al. (2004), which shows that the observed spin-down is negligibly affected by accelerations (it is in the outskirts of the cluster as is shown in Anderson 1993). The following pulsars use distance estimates that are not taken from the values given in the ATNF pulsar catalog: PSR J1017−7156 (updated parallax distance provided by R. M. Shannon 2016, private communication), PSR J1418−6058 (distance to more distant association in Yadigaroglu & Romani 1997), PSR J1813−1246 (lower limit on distance from Marelli et al. 2014), PSR J1823−3021A (distance for NGC 6624 in Valenti et al. 2007), PSR J1824−2452A (distance for M28 in Rees & Cudworth 1991), PSR J1826−1256 (lower distance range from Wang 2011; Voisin et al. 2016), PSRs J1910−5959A, C, and D (distances of 4.45 kpc calculated from the distance modulus to NGC 6752 in Table 4 of Gratton et al. 2003), PSR J2129+1210C (McNamara et al. 2004), and PSR J2234+06 (P. C. C. Freire 2016, private communication).
[a] The pulsar's spin-down is corrected for proper motion effects.
[b] The pulsar's spin-down is calculated using a characteristic spin-down age of 10^9 years and a braking index, n, of 5 (i.e., braking due to gravitational radiation).
[c] Uses a restricted prior on orientation parameters (see Appendix B).

(This table is available in its entirety in machine-readable form.)

where $H_{S/N_{H1/L1}}$ represents the hypothesis of our signal model/ noise in the given detector. This gives a ratio

$$\mathcal{O}_{S/I} = \frac{p(\boldsymbol{d}|H_S)p(H_S)}{p(\boldsymbol{d}|H_{N_1})p(H_{N_1}) + p(\boldsymbol{d}|H_{N_2})p(H_{N_2}) + p(\boldsymbol{d}|H_{N_3})p(H_{N_3}) + p(\boldsymbol{d}|H_{N_4})p(H_{N_4})}. \tag{12}$$

We choose the five hypothesis priors ($p(H_S)$, $p(H_{N_1})$, $p(H_{N_2})$, $p(H_{N_3})$, and $p(H_{N_3})$) such that they have equal probabilities, and they therefore factorize out of the calculation.[170] Such a probability ratio (i.e., the odds) obviously penalizes single detector detections, in which one detector may be considerably more sensitive than the other.

Appendix B
Orientation Angle Priors

For several pulsars in our search, there are observations of their PWN. Under the assumption that a pulsar's orientation is

aligned with its surrounding nebula, we can use the fits to the pulsar orientation given in Ng & Romani (2004, 2008) as

restricted priors on ψ and ι. For the Bayesian and $5n$-vector methods, the prior probability distributions on ψ and ι are Gaussian distributions based on the PWN fits, while the $\mathcal{G}$-statistic uses a δ-function prior at the best-fit value. Table 3 shows the means and standard deviations used for the parameter priors. In general, these are taken from Table 2 of Ng & Romani (2008), where Ψ is equivalent to our ψ, and ζ is equivalent to our ι.[171] Statistical and systematic uncertainties are added in quadrature (for non-symmetric uncertainties, the larger value is used). For the Crab pulsar and PSR J0205 +6449, Ng & Romani (2008) give fits to the inner and outer PWN torii, so in these cases our mean value is the average of the inner and outer fits, and the quadrature-combined

---

[170] The hypothesis H_{N_1} contains all the other hypotheses as its subsets, but within it the other hypotheses will all be downweighted by their tiny prior volumes in comparison to the full volume. Therefore, to provide more weight to the alternative noise hypotheses, we explicitly include them with equal weight.

[171] ψ can be rotated by integer numbers of $\pi/2$ radians and still give signals within our search parameter space, although for each rotation any signal would have ϕ_0 equivalently rotated by π radians.

systematic and statistical errors for each are combined via $\sigma = \sqrt{(\sigma_{\mathrm{inner}}/2)^2 + (\sigma_{\mathrm{outer}}/2)^2}$.

When these restricted priors were used in the previous analyses of Aasi et al. (2014), there has been an implicit (and at the time unrealized) assumption about the rotation of the star. As noted in Jones (2015), constraining ι and ψ to particular values implicitly forces a rotation direction on the signal, while the PWN observations (or indeed the electromagnetic timing observations) give us no knowledge of the actual rotation direction. To incorporate this unknown rotation direction in the search, while maintaining the convenient minimal range in ψ of $\pi/2$ radians, there must be a bimodal distribution on ι with the additional mode at $\pi - \iota$ radians. The mean and standard deviations of Gaussian prior distributions used for ψ and the two modes for ι are given in Table 3.

References

Aasi, J., Abadie, J., Abbott, B. P., et al. 2014, ApJ, 785, 119
Aasi, J., Abbott, B. P., Abbott, R., et al. 2015, PhRvD, 91, 022004
Abadie, J., Abbott, B. P., Abbott, R., et al. 2011, ApJ, 737, 93
Abbott, B. P., Abbott, R., Abbott, T. D., et al. 2016a, arXiv:1602.03845
Abbott, B. P., Abbott, R., Abbott, T. D., et al. 2016b, PhRvL, 116, 241103
Abbott, B. P., Abbott, R., Abbott, T. D., et al. 2016c, PhRvL, 116, 061102
Abbott, B. P., Abbott, R., Abbott, T. D., et al. 2016d, LRR, 19, 1
Abbott, B. P., Abbott, R., Acernese, F., et al. 2010, ApJ, 713, 671
Abbott, B., Abbott, R., Adhikari, R., et al. 2007, PhRvD, 76, 042001
Abbott, B., Abbott, R., Adhikari, R., et al. 2008, ApJL, 683, L45
Abdo, A. A., Ajello, M., Allafort, A., et al. 2013, ApJS, 208, 17
Anderson, S. B. 1993, PhD thesis, California Institute of Technology
Antil, H., Field, S. E., Herrmann, F., Nochetto, R. H., & Tiglio, M. 2013, JSCom, 57, 604
Archibald, R. F., Gotthelf, E. V., Ferdman, R. D., et al. 2016, ApJL, 819, L16
Astone, P., Colla, A., D'Antonio, S., Frasca, S., & Palomba, C. 2012, JPCS, 363, 012038
Astone, P., D'Antonio, S., Frasca, S., & Palomba, C. 2010, CQGra, 27, 194016
Biwer, C., Barker, D., Batch, J. C., et al. 2016, arXiv:1612.07864
Bonazzola, S., & Gourgoulhon, E. 1996, A&A, 312, 675
Canizares, P., Field, S. E., Gair, J. R., & Tiglio, M. 2013, PhRvD, 87, 124005
Condon, J. J., & Ransom, S. M. 2016, Essential Radio Astronomy (Princeton: Princeton Univ. Press)
Cordes, J. M., & Lazio, T. J. W. 2002, arXiv:astro-ph/0207156
Cutler, C. 2002, PhRvD, 66, 084025
Dupuis, R. J., & Woan, G. 2005, PhRvD, 72, 102002
Freire, P. C. C., Abdo, A. A., Ajello, M., et al. 2011, Sci, 334, 1107
Gratton, R. G., Bragaglia, A., Carretta, E., et al. 2003, A&A, 408, 529
Haskell, B., Samuelsson, L., Glampedakis, K., & Andersson, N. 2008, MNRAS, 385, 531
Hobbs, G. B., Edwards, R. T., & Manchester, R. N. 2006, MNRAS, 369, 655
Jaranowski, P., & Królak, A. 2010, CQGra, 27, 194015
Jaranowski, P., Królak, A., & Schutz, B. F. 1998, PhRvD, 58, 063001
Jeffreys, H. 1998, Theory of Probability (3rd ed.; Oxford: Oxford Univ. Press)
Johnson, T. J., Guillemot, L., Kerr, M., et al. 2013, ApJ, 778, 106
Johnson-McDaniel, N. K. 2013, PhRvD, 88, 044016
Johnson-McDaniel, N. K., & Owen, B. J. 2013, PhRvD, 88, 044004
Jones, D. I. 2015, MNRAS, 453, 53
Keitel, D., Prix, R., Papa, M. A., Leaci, P., & Siddiqi, M. 2014, PhRvD, 89, 064023
Knispel, B., & Allen, B. 2008, PhRvD, 78, 044031
Lyne, A. G., Jordan, C. A., Graham-Smith, F., et al. 2015, MNRAS, 446, 857
Manchester, R. N., Hobbs, G. B., Teoh, A., & Hobbs, M. 2005, AJ, 129, 1993
Marelli, M., Harding, A., Pizzocaro, D., et al. 2014, ApJ, 795, 168
McNamara, B. J., Harrison, T. E., & Baumgardt, H. 2004, ApJ, 602, 264
Middleton, H., Del Pozzo, W., Farr, W. M., Sesana, A., & Vecchio, A. 2016, MNRAS, 455, L72
Ng, C.-Y., & Romani, R. W. 2004, ApJ, 601, 479
Ng, C.-Y., & Romani, R. W. 2008, ApJ, 673, 411
Owen, B. J. 2005, PhRvL, 95, 211101
Owen, B. J. 2006, CQGra, 23, S1
Palomba, C. 2000, A&A, 354, 163
Palomba, C. 2005, MNRAS, 359, 1150
Pitkin, M. 2011, MNRAS, 415, 1849
Pitkin, M., Gill, C., Jones, D. I., Woan, G., & Davies, G. S. 2015, MNRAS, 453, 4399
Pitkin, M., Gill, C., Veitch, J., Macdonald, E., & Woan, G. 2012, JPCS, 363, 012041
Prix, R., & Krishnan, B. 2009, CQGra, 26, 204013
Rees, R. F., & Cudworth, K. M. 1991, AJ, 102, 152
Ridolfi, A., Freire, P. C. C., Torne, P., et al. 2016, MNRAS, 462, 2918
Scargle, J. D. 1998, ApJ, 504, 405
Shklovskii, I. S. 1969, AZh, 46, 715
Skilling, J. 2006, Bayesian Anal., 1, 833
Valenti, E., Ferraro, F. R., & Origlia, L. 2007, AJ, 133, 1287
Veitch, J., & Vecchio, A. 2010, PhRvD, 81, 062003
Veitch, J., Raymond, V., Farr, B., et al. 2015, PhRvD, 91, 042003
Voisin, F., Rowell, G., Burton, M. G., et al. 2016, MNRAS, 458, 2813
Wang, W. 2011, RAA, 11, 824
Yadigaroglu, I.-A., & Romani, R. W. 1997, ApJ, 476, 347